
# Impact of Wind Driven Variability on Sea Surface Temperature and Ocean Colour in False Bay

**Sian Seymour**

SMRSIA001

**Supervisors:**

Dr Marjolaine Krug

Dr Marie Smith

Dr Alexis Mouche

Prof Mathieu Rouault



**A thesis presented in partial fulfilment of the requirements for the degree of Master of Sciences in Applied Ocean Sciences**

February 2019

Department of Oceanography, University of Cape Town

The financial assistance of the National Research Foundation (NRF) towards this research is hereby acknowledged.

Opinions expressed, and conclusions arrived at, are those of the author and are not necessarily to be attributed to the NRF.

**ABSTRACT**

False Bay is the largest true bay in South Africa and is an important area for conservation, the local fishing industry and marine based recreational activities. A large amount of studies, both recent and historical, have been carried out on the biology of the bay, but studies on the physics of the bay are very few in comparison. In this study high resolution satellite imagery is used to investigate wind variability and its impact on sea surface temperature (SST) and chlorophyll concentration (Chl-a) variability within False Bay and the Cape Peninsula region. High resolution (1 km) coastal winds derived from the Sentinel-1 satellite Synthetic Aperture Radar (SAR) show that winds are strongly influenced by topography under the predominantly south-easterly wind regime. The Hottentots-Holland mountain range and Cape Peninsula mountain range create wind shadows as well as areas of increased wind speed within False Bay and west of the Cape Peninsula. Our observations also show that global atmospheric models, such as ECMWF, are not able to capture the spatial variability in the wind fields driven by the orography. Analyses of the SST and ocean colour imagery show that wind shadows are generally associated with warmer surface waters and higher Chl-a. In contrast, regions of enhanced wind speeds show colder surface waters and decreased chlorophyll concentration. Our results suggest that spatial variation in the horizontal wind fields have direct and significant impact on the water properties within False Bay. This study highlights the need for high resolution wind observations and simulations to force regional oceanic models of False Bay and the Cape Peninsula region.

**PLAGIARISM DECLARATION**

1. I know that plagiarism is wrong. Plagiarism is to use another's work and pretend that it is one's own.
2. I have used the Harvard convention for citation and referencing. Each contribution to, and quotation in, this thesis from the work(s) of other people has been attributed, and has been cited and referenced.
3. This thesis is my own work, and is in my own words (except where I have attributed it to others)
4. I have not allowed, and will not allow, anyone to copy my work with the intention of passing it off as his or her own work.
5. I acknowledge that copying someone else's assignment or essay, or part of it, is wrong, and declare that this is my own work

Signed: Signed by candidate Date: 2019/02/08

**ACKNOWLEDGMENTS**

I would like to sincerely thank the following people for their help in making this project a reality:

- Dr Marjolaine Krug and Dr Marie Smith for their guidance and support, for always being available when I needed some help and for always providing me with feedback as soon as possible. You really helped to make this year more enjoyable than stressful
- Prof Mathieu Rouault for his guidance and assistance in finding this project as well as finding funding
- Dr Alexis Mouche and IFREMER for the processing of the SAR data
- My classmates for making this year both memorable and enjoyable
- NRF and Nansen-Tutu Centre for providing me with the funds needed to complete this year of study
- My amazing parents who have always pushed me to be my best
- Nik Basting, for his love, support and understanding, especially during the stressful times

# CONTENTS

## TABLES



## FIGURES

## 1. INTRODUCTION

False Bay and the Cape Peninsula (Fig. 2.1) are important areas both on a conservational level as well as on a human level. The bay is home to a rich and diverse marine and coastal life, and contains important fishing grounds. The region is also home to the largest naval base in the country, contains important harbours and plays host to a variety of recreational activities (Gründlingh & Largier, 1991; van Ballegooyen, 1991). Understanding the wind regime of this area as well as how it can affect other ocean dynamics is therefore important for this continued co-existence between man and sea. Historically wind data has not been very abundant or of adequate spatial resolution, especially in coastal regions (Holt, 2004). Wind data along the coast has often been collected through the use of land-based anemometers, however, these devices are not abundant enough to provide sufficient data for a true representation of wind variability over larger areas and further offshore (Dagestad *et al*., 2013). *In situ* data collected on the ocean may provide a better understanding of winds away from the coastline, but due to the large expanse of the ocean, and limited resources such as time and money, these data do not often provide a spatial resolution high enough to truly represent spatial wind variability over the ocean. Winds are a fundamental driver of many ocean dynamics, such as circulation and upwelling, which in turn can affect other dynamics such as SST and biology (Jacobson, 2014; Gründlingh & Largier, 1991; Jury *et* al., 1985a; Jury *et* al., 1985b; Pitcher *et al*., 2010). Due to the lack of accurate high-resolution wind in False Bay, these dynamics and their variability have not yet been resolved opening up areas of study where more research and more reliable data are required.

Winds are a primary driver of ocean variability, both at the coast and offshore. Sea surface temperature (SST) and orography are two significant factors that can influence coastal winds (Chelton *et al*., 2004; Small *et al*., 2008; Renault et al., 2016). Studies have shown that there is often a positive correlation between SST and winds at ocean fronts due to the influence of temperature changes on the static stability of the marine atmospheric boundary layer (MABL) and vertical turbulence mixing (Nonaka & Xie, 2003; O'Neill *et al*., 2003; Chelton *et al*., 2004; Tokinaga *et al*., 2005). However, in coastal areas, orographic effects are often the dominant influencer of wind variability (Chelton *et al*., 2004). This seems to be the case for False Bay and the larger Cape Peninsula area, where atmosphere-orography interactions dominate over ocean-atmosphere ones (Jury, 1985; Jury *et* al., 1985a; Jury *et* al., 1985b; Jury, 1987; Wainman *et al*., 1987; Jury, 1988).

Currently, satellite observations are the primary source for information on ocean winds. These satellites, known as scatterometers and radiometers, use microwave sensors to measure derived wind speeds from wind-induced ocean surface roughness (Long & Skouson, 1996). The introduction of these satellites has allowed for wind speed measurements over larger areas but at a coarse resolution of 25 to 50 km. This low spatial resolution has resulted in a lack of observations near the coast due to land contamination (Holt, 2004).

Wind information can also be retrieved from Synthetic Aperture Radar (SAR) observations from satellites (Dagestad *et al*., 2013). Similar to scatterometers, SARs use active microwave radars to measure sea surface roughness, however, at a significantly higher resolution of 500 m to 1 km (Dagestad *et al*., 2013). This high spatial resolution and the resultant decrease in land contamination allows for the observation of fine scale wind variability and the possibility to examine wind speeds in coastal regions (Dagestad *et al*., 2013).

## 1.1. Goals and objectives

### 1.1.1. Problem formulation

The use of high-resolution SAR wind speed data could help to observe previously unresolved wind variability near the coast, such as in False Bay and the Cape Peninsula, where small scale variability can occur due to effects of the nearby topography (Jury *et* al., 1985a; Jury *et* al., 1985b Jury, 1987). These orographic effects could in turn influence other ocean dynamics near the coast (Jury, 1985; Jury *et* al., 1985a; Jury *et* al., 1985b; Pitcher *et al*., 2010). Within False Bay, modelled circulation obtained with regionally uniform winds resulted in a very different circulation pattern than that obtained with spatially varying winds (Jacobson, 2014). Winds are a primary driver of ocean variability within the region and knowledge on the wind regime is essential for our understanding of the ocean circulation and other ocean dynamics. Upwelling systems such as False Bay and the Benguela as a whole are susceptible to Harmful Algal Blooms (HABs). False Bay has been recognised as having a high phytoplankton biomass with the time of these HABs largely influenced by wind stress fluctuations (Pitcher *et al*., 2010). Previous studies focusing on wind variability within the False Bay region have been limited due to a lack of observations. Most of our understanding of the variability in the wind field and SST of False Bay and the Cape Peninsula region has been derived using either *in situ* point observations or aircraft surveys which provided wind fields at a spatial resolution of at best 10 km and at an altitude of 100 m (Jury, 1985; Jury *et* al., 1985a; Jury *et* al., 1985b; Jury, 1987; Jury, 1988).

Coastal areas are of great importance as this is where the majority of human interaction with the sea takes place. An improved understanding of the wind regime and ocean dynamics may help improve human-ocean interactions in the bay, such as fishing and recreational activities, as well as current and future conservation efforts taking place within False Bay and the Cape Peninsula.

This study exploits high resolution 1 km wind observations from the SAR on board the Sentinel-1 satellites to improve our understanding of coastal winds within the False Bay and Cape Peninsula oceanic area. Such high-resolution satellite data have never been used to explore ocean surface winds within this region.

### 1.1.2. Research questions

There is a gap in the literature focusing on high resolution coastal wind variability and wind forcing in False Bay and the Cape Peninsula. After a review of the existing literature and current real-world problems, the following research questions were developed:

- Can the Sentinel-1 SAR improve our capabilities to observe winds over the Cape Peninsula oceanic regions?
- What is the spatial wind variability across False Bay and the Cape Peninsula during the dominant south-easterly (SE) wind regime?
- What is the response of SST and chlorophyll concentrations (Chl-a) to this wind forcing?

### 1.1.3. Approach

The approach to answer these research questions was to:

1. Characterise spatial variability in wind speed over False Bay and the Cape Peninsula during the dominant SE wind regime and interpret orographic influence on this variability
2. Determine if small scale orographic effects on wind speed are captured in high resolution (9 km) atmospheric models (ECMWF)
3. Map and quantify magnitude and spatial extent of regions of increased/ decreased wind (wind shadows and regions of intensified wind)
4. Identify areas of upwelling and possible retention zones within False Bay
5. Explore the response of SST and Chl-a to wind forcing
6. Explore seasonal variation in wind, SST and Chl-a in areas of upwelling and wind shadow

This study uses selected case studies where high-resolution data for wind speed, SST and Chl-a were all available. For each case study day, maps of wind speed, SST and Chl-a were created to provide visual representations of their variability within the study area. The difference between SAR derived wind speeds and high-resolution ECMWF modelled wind speed was observed to show biases in global atmospheric models near the coast and to quantify the extent and magnitude of spatial wind variability. Ekman pumping was calculated to gain insight into the impact of wind driven vertical motions on the circulation within False Bay. Regional maps as well as transects taken across the northern section of the Cape Peninsula and within False Bay were used to determine if any co-variability occurred between wind speed, SST and Chl-a. The impact of the wind's spatial variability on the SST and Chl-a over longer time scales was investigated using time-series extracted over upwelling zones and wind shadows zones within False Bay and off the Cape Peninsula.

## 1.2. Document structure

In Chapter 2, a literature review is presented covering current knowledge on wind variability and wind forcing within False Bay and the Cape Peninsula. This is followed by Chapter 3 where methods and data analysis are discussed. In Chapter 4, the results of this study are presented. Lastly, the outcomes

of the study are discussed in Chapter 5 and presented in context with current knowledge and understanding on the topic.

## 2. LITERATURE REVIEW

### 2.1. Study area

Despite its misleading name, False Bay is the largest true bay in South Africa. It is rectilinear in shape, with an area of roughly 1000 km$^2$ and a coastline that stretches for 146 km (Spargo, 1991; van Ballegooyen, 1991). It is situated between latitudes 34 and 35 ˚S and longitudes 18 and 19 ˚E with its mouth facing south towards the South Atlantic Ocean (Spargo, 1991; van Ballegooyen, 1991). A unique aspect of False Bay is its surrounding topography. The bay is flanked on the west by the mountains of the Cape Peninsula ending at Cape Point, and on the east by the Kogelberg, an extension of the Hottentots-Holland mountain range, ending at Cape Hangklip (Shannon *et al.*, 1991; Spargo, 1991)(Fig. 2.1). A low-lying area of mostly 10 m above sea level, known as the Cape Flats, is found to the north of the bay (Spargo, 1991) (Fig. 2.1). Over the past 50 years this northern boundary of False Bay has seen a rapid increase in human population, resulting in an increase in human pressure on the area, specifically in terms of waste disposal and recreational activities (Spargo, 1991). Although False Bay is part of the Benguela upwelling regime, it is rather anomalous in terms of its oceanography in comparison to other areas on the west coast of South Africa. This is due to its unique geography and topography and the resulting orographic effects these have on the wind regime (Jury, 1985; Jury *et* al., 1985a; Jury *et* al., 1985b; Jury, 1988; Wainman *et al.*, 1987; Shannon *et al.*, 1991).


Figure 2.1. The topography surrounding False Bay and the Cape Peninsula. A) Kogelberg Mountain Range, B) Cape Hangklip, C) Cape Flats, D) Cape Point, E) Table Bay, F) Cape Peninsula Mountain Range. (Source: SRTM Team NASA)

### 2.2. Synoptic wind regime

False Bay and the Cape Peninsula are dominated by a predominantly SE wind regime. These winds are created by a pressure gradient between the South Atlantic Anticyclone (SAA) and continental lows over South Africa (Jury, *et al.*, 1985b; Wainman, *et al.*, 1987, Risien *et al.*, 2004). These atmospheric

lows are a result of the fragmentation of large atmospheric Rossby waves in higher latitudes (Gründlingh & Largier, 1991). The eastward movement of these midlatitude troughs and ridges creates a pulsing in this pressure gradient (Jury, 1987, Jury, 1991). Westerly winds and fronts associated with these low-pressure systems pass over southern Africa during winter and pass south of the continent during summer (Gründlingh & Largier, 1991). Coastal lows created as a result of these frontal passages are formed off the west coast of southern Africa. The passage of these low-pressure systems, as well as the SAA, creates temporal wind variability in the wind regime of False Bay, resulting in four distinct wind phases (Gründlingh & Largier, 1991). These phases occur chronologically as the south-westerly (SW) regime, the deep SE regime, the shallow SE regime and the north-westerly (NW) regime (Jury, 1980; Diab & Garstang, 1984; Jury, 1991) (Fig. 2.2).

The first of these phases, the SW regime, occurs with the leading edge of a ridging SAA and follows the passage of a cold front. The formation of continental lows and the southward ridging of the SAA leads into the deep SE regime. Here winds flowing over the Hottentots-Holland mountains and Cape Hangklip are vertically compressed by the inversion layer and accelerate over False Bay. The formation of coastal lows off the west coast of South Africa and the further southward movement of the SAA forms the shallow SE regime. As the inversion layer decreases, winds are prevented from flowing over high mountain ridges and areas of wind shadow in lee of the mountains are created. Wind acceleration around Cape Hangklip and Cape Point also occur as winds are deflected seaward. Finally, the NW regime follows the passage of coastally trapped lows and signals the approach of a cold front. This results in poleward flowing winds which then curl around Table Mountain and flow in a north west direction over False Bay (Jury, 1991). Wind variability is also affected by seasonal changes in wind intensity, where southerly winds dominate during summer months but a northerly shift in the position of the SAA in winter results in an increase in NW winds and a reduction in the duration of the following south-easter (Jury, 1991; Gründlingh & Largier, 1991).

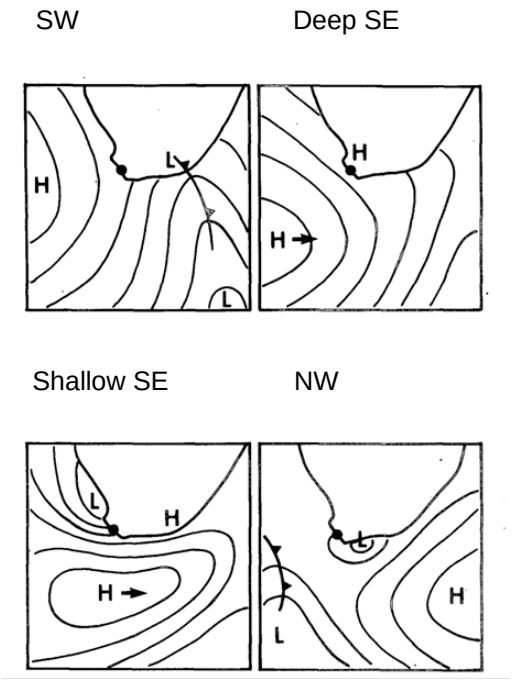


Figure 2.2. A schematic showing the four phases of the synoptic weather cycle, the south-westerly regime (SW) (top left), the deep south-easterly (SE) regime (top right), the shallow south-easterly regime (bottom left) and the north-westerly (NW) regime (bottom right), which influence wind flow over False Bay and the Cape Peninsula. From Jury (1987).

## 2.3. Drivers of variability in coastal winds

### 2.3.1. SST

Variability of ocean winds is often influenced by ocean surface temperatures and when it comes to wind and SST many studies have shown that there is a positive correlation between the two at ocean fronts. This is true for the Kuroshio Extension (Nonaka & Xie, 2003), the Gulf Stream (Chelton *et al*., 2004), the Brazil-Malvinas Confluence (Tokinaga *et al*., 2005) and the Agulhas Current (O'Neill *et al*., 2003).

This co-variability is a result of an air-sea interaction, as sharp changes in SST influence the air-sea heat flux in the marine atmospheric boundary layer (MABL) (Chelton *et al*., 2004; Small *et al*., 2008). A sharp increase in SST results in a decrease in the static stability of the MABL, enhancing vertical turbulence mixing and bringing fast moving air down to the ocean surface (Nonaka & Xie, 2003; Chelton *et al*., 2004). The opposite occurs for a decrease in SST as cold water stabilizes the MABL.

This correlation has also been observed in coastal areas. In a study by Jin *et al*. (2009) mesoscale air-sea coupling was observed in an eastern boundary upwelling current system using the Regional Oceanic Modeling Systems (ROMS). A decrease in wind stress near the coast was observed, corresponding to colder nearshore SST. This air-sea coupling has been observed in other coastal

areas, such as Bodega Bay in California (Dorman *et al*., 2006) and the California Current System (CCS) (Chelton *et al*., 2007), as well as in other ocean models (Perlin *et al*., 2007).

2.3.2. Orography

Besides SST fronts, orography is another factor than can influence coastal winds. In the CCS a decrease in winds near the coast is not only a result of SST fronts caused by cooler upwelled water, but this wind drop-off is also influenced by coastal topography (Renault et al., 2016). Atmospheric simulations over this area showed that there is both spatial and seasonal variability in the extent and intensity of this drop off due to orographic effects (Renault et al., 2016). In addition to wind drop-offs and wind shadows, coastal topography can also result in wind accelerations. Wind jets as a result of orography and shallow inversion layers have been described in several coastal regions including central California (Doyle, 1997) and in the west coast of South Africa (Jury *et* al., 1985a; Jury *et* al., 1985b; Jury, 1987; Jury, 1988). Variable coastal topography does not only influence wind speed but wind direction as well, with high mountain ridges and capping inversion layers resulting in the deflection of coastal winds (Smith, 1982; Jury 1991). Although the co-variability between SST and wind speed is most often observed at a mesoscale level, this positive correlation is not always observed on smaller scales around islands and near the coast (Chelton *et al*., 2004). Chelton *et al*., (2004) used four-year global averages of near-surface wind speeds to plot wind stress curl and wind stress divergence over global SST fronts. Although positive correlation between wind speed and SST was observed over open ocean, near the coast small scale variability in the divergence field was attributed to orographic effects (Fig. 2.3).

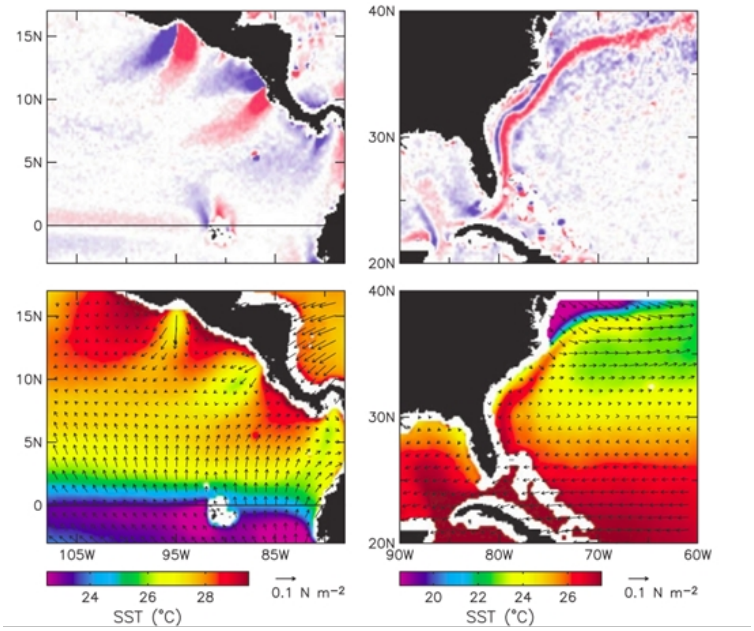


Figure 2.3. A 14-year average (August 1991 – July 2003) of wind stress curl (top panel) over the eastern North Pacific (left) and western North Atlantic (right) derived from 25 km resolution winds taken from the QuikSCAT scatterometer, and

a 14-year average of SST (bottom panel) derived from Tropical Rainfall Measuring Mission Microwave Imager (TMI) images. Left panels in the figure show the effects of topography on wind curl and SST whereas right panels show the effect of temperature fronts on winds. From Chelton *et al. (*2004*).*

### 2.3.3. Wind variability in False Bay

Due to the lack of long-term and high spatial resolution measurements over False Bay, there is little understanding of the wind variability within the bay itself. However, short term studies have brought some insight into the variability of wind speed and direction.

Several studies have been performed along the west-coast and south-west coast of South Africa using aerial survey data (Jury, 1985; Jury *et* al., 1985a; Jury *et* al., 1985b; Jury, 1987; Jury, 1988). Jury (1987) used case studies to describe the mesoscale patterns in each of the four wind regimes (SW, deep SE, shallow SE, NW) over the region between 30 and 35 ˚S during the summer season. During the SW regime winds were described as flowing relatively uniformly over the False Bay. During the SE regimes' winds were influenced by a shallow inversion layer and were vertically compressed over mountain ridges resulting in wind accelerations over Cape Hangklip and Cape Point. Additionally, a capping inversion layer created wind shadows and slower wind speeds within False Bay and north west of the Cape Peninsula in lee of the mountain ridges. During this time wind speed was at its maximum at Cape Point and Cape Hangklip where they were almost double that of winds in the bay (Jury, 1987). The wind speed and SST observed during a shallow SE regime for the Jury (1987) study is shown in Figure 2.4. Finally, during the NW phase wind speed and direction was mostly homogenous over False Bay (Jury, 1987). Similar studies focusing only on the Cape Peninsula shows wind acceleration over the southern portion of the Peninsula and a wind shadow in lee of the northern portion of the peninsula mountains due to vertical compression and orographic obstruction during shallow SE winds (Jury *et al*., 1985a; Jury *et al*., 1985b). Wainman *et al.* (1987) used wind data from anemometers from six set locations around False Bay collected for five months (February to May) at three-day intervals. Mean summer winds were found to be predominantly easterly at the mouth of the bay and along the eastern shore, whereas winds were more southerly over the north western region of the bay. In this study, a one-day synoptic survey of the SE wind regime was also created using boat surveys. Results showed a noticeable wind shadow in the eastern region of the bay.

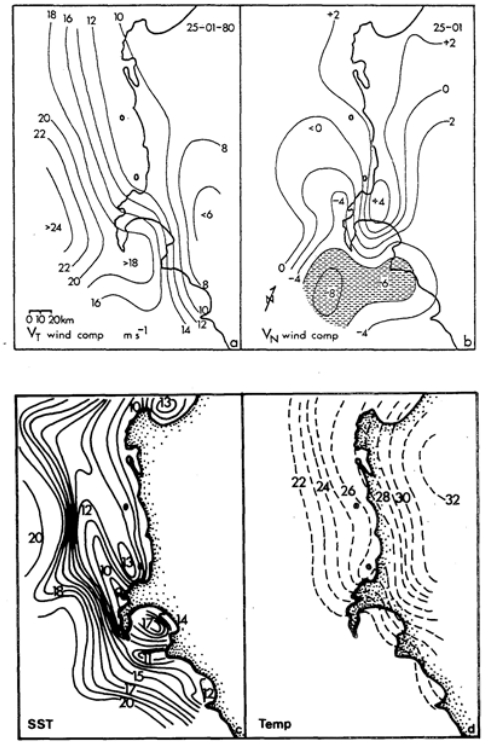


Figure 2.4. a) The along shore wind component, b) across-shore wind component, c) sea surface temperature (SST) and d) air temperature at 150 m derived from aerial survey data during shallow south-easterly winds on 25 January 1980. From Jury (1987).

Most of our understanding of the small-scale wind variability within False Bay and the Cape Peninsula comes from the aerial survey studies by Jury (Jury *et* al., 1985a; Jury *et* al., 1985b; Jury, 1987; Jury, 1988). These studies derived wind speed from aircraft drift at an altitude of 150 m with a positioning accuracy of about 500 m resulting in a spatial resolution of at best 10 km (Jury *et al*., 1985b). Due to these methods there could be significant error in the wind speed and direction and results may not be an accurate representation of wind variability within the region. Additionally, these studies only provide information along transects across the bay rather than a true synoptic view of wind variability over the bay, which could be provided by satellite data. Currently, there are eight South African Weather Service (SAWS) automated weather stations (AWS) within the area. Five of these are coastal, located at Cape Point, Slangkop, Cape Town Royal Yacht Club, Strand and Robben Island, and three are located inland at Kirstenbosch Botanical Gardens, the South African Astronomical Observatory and Molteno Reservoir (South African Weather Service, SAWS). Data from these weather stations were not used in this study as the weather station data can only provide data for those specific inland points and can not support our analysis of the wind variability across the oceanic area. Overall, there is a great lack in studies using high resolution wind data, not just in False Bay but in coastal regions in general.

## 2.4. Impact of coastal winds on the environment

Coastal regions are largely influenced by winds due to interactions between the land-sea interface. Coastal topography can create wind variability due to orographic effects on the wind regime, such as wind diversions, accelerations and blockages. Various wind flow phenomena can arise, such as mountain waves, lee waves and rotors, downslope windstorms, gap winds and barrier jets, all of which are discussed in Jackson *et al*. (2013). These orographic effects on the variability of the wind regime can influence other coastal ocean dynamics, such as circulation, SST and biology.

### 2.4.1. Circulation

Winds are the primary driving force of currents within False Bay, affecting both ocean temperature and biology within these waters (Wainman *et al*., 1987; Jacobson, 2014). Studies have suggested a predominantly cyclonic flow within the bay driven by SE winds (Gründlingh & Largier, 1991). This clockwise circulation has been observed on several occasions in different studies including studies using “dye bombs” (Atkins, 1970a), deep current meter moorings placed within the bay (Wainman *et al*., 1987) and a moored current meter array across the mouth of False Bay (Gründlingh *et al*., 1989). However, a numerical model study by Van Foreest & Jury (1985) suggested an anticlockwise flow under summer conditions, however, it should be noted that this study used a very simple model with various limitations such as the use of an isolated wind regime (Gründlingh *et al*., 1989; Gründlingh & Largier, 1991)

More recently, a numerical modelling experiment using the Regional Ocean Modelling System (ROMS) forced by surface winds during summer months was performed to explore circulation and SST in False Bay (Jacobson, 2014). Wind forcing data were derived using Conformal-Cubic Atmospheric Model (CCAM) wind outputs of a spatial resolution of roughly 1 km (Jacobson, 2014). Within the study two runs were performed, a uniform run employing spatially averaged winds and a varying run employing spatially varying winds. Besides the spatial wind variability, the runs were identical (Jacobson, 2014). Under uniform winds anticyclonic flow within the bay was observed with inflow at Cape Hangklip and out flow at Cape Point. Cool SST occurred along the eastern shores, signalling upwelling and the highest temperatures were found in the north-western corner of the bay where waters were relatively calm (Fig. 2.5A) (Jacobson, 2014). Under the spatially varying wind field, circulation was cyclonic, with an anticyclonic feature evident in the north east. Inflow occurred at Cape Point and outflow at Cape Hangklip (Fig 2.5B). Low SSTs were found in the southern half of the bay and warmer SSTs in the northern half. Jacobson (2014) found that circulation and SST were substantially different between the runs, suggesting that wind variably has a large effect on the variability of circulation and subsequently SST in False Bay.

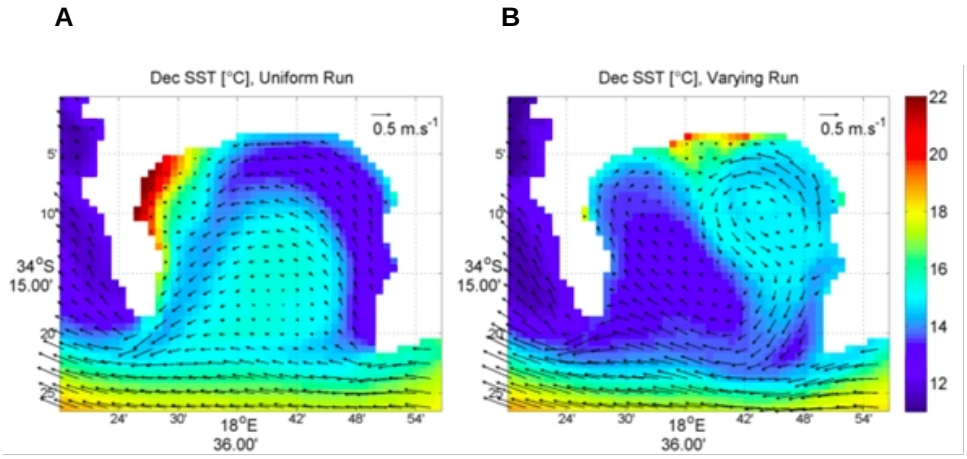


Figure 2.5. Maps showing a climatological monthly means for modelled sea surface temperatures (SST) with modelled surface ocean currents over laid as surface flow vectors for the years 2 – 6 from a 6 year Regional Ocean Modelling System (ROMS) run forced by A) uniform and B) varying winds. The length of the arrows depict the current speed and the orientation depicts the direction of flow. From Jacobson (2014).

### 2.4.2. SST

As previously mentioned, strong temperature fronts can drive changes in wind speeds. On the other hand, variable winds can also influence ocean surface temperatures in coastal regions through ocean driven processes such as Ekman upwelling and retention. Alongshore winds create offshore Ekman transport when Coriolis forces are directed away from the coast and move surface waters seaward, bringing cold nutrient rich bottom water to the surface (Wang *et al*., 2015). This often result in SST fronts between the cold upwelled coastal waters and the warmer offshore waters (Wang *et al*., 2015). These upwelling fronts have been observed in Eastern Boundary Current Systems all over the world, including the California Current System, the Benguela Current System and the Canary Current System (Wang *et al*., 2015), as well as in other coastal regions such as southern Madagascar (Ramanantsoa *et al*., 2018) and the southern Caribbean upwelling system (Rueda-Roa & Muller-Karger, 2013). These SST fronts have been shown to be most prominent near the coast and decrease in probability with distance from the shore (Wang *et al*., 2015). Additionally, these frontal features can be influenced by the orographic effects caused by surrounding topography and other mesoscale dynamics (Castelao *et al*., 2005; Wang *et al*., 2015).

Winds are the primary driving force of ocean variability along the west coast and south west coast of South Africa (Jury, 1985; Jury *et* al., 1985a; Jury *et* al., 1985b; Jury, 1987; Wainman *et al*., 1987; Jury, 1988). However, there is still a deficit in the amount of studies on the SST response to wind forcing within False Bay. Early studies looking at SST were performed by Cram (1970) using airborne radiation thermometry and Atkins (1970a; 1970b) using bathythermographs at several stations on several cruises. The main outcome of these studies was the observation of an upwelling plume off Cape Hangklip during SE winds and a difference between mean warm summer (19 ˚C) and cold winter (15 ˚C) ocean

surface temperatures. This wind induced upwelling off Cape Hangklip has been observed on several separate occasions (Cram, 1970; Shannon *et al.*, 1983; Jury 1987; Jury, 1991; Lutjeharms *et al.*, 1991) with a smaller upwelling plume also being recorded off Gordon's Bay (Jury, 1987). Once the winds subsided and upwelling stopped, these plumes were found to move north-westward into the bay and dissipate after a few days due to vertical mixing (Jury, 1987; Gründlingh & Largier, 1991) with Wainman *et al.*, (1987) observing a decrease of SST in the bay that correlated with an increase in SE winds.

Studies using aerial surveys have been performed to look at wind driven SST variability along the west coast and south west coast of South Africa (Jury, 1985; Jury *et* al., 1985a; Jury *et* al., 1985b; Jury, 1987; Jury, 1988). Jury (1988) used aircraft-based observations of wind speed and SST data and compared non-upwelling and upwelling scenarios off Cape Hangklip. The wind speeds and SST were derived from aircraft drift and the infrared observations from aerial surveys flown at 150 m altitude. NW winds were dominant during the non-upwelling scenario where as predominantly SE winds blew during the upwelling scenario. Observable upwelling plumes of cold water spreading north-westward off Cape Hangklip corresponded to areas of stronger wind speed during the SE scenario. Similar results were observed off the Cape Peninsula during SE winds with a strong cold upwelling tongue stretching north-westward off the south of the peninsula, corresponding to areas of accelerated wind speeds (Jury, 1985; Jury *et* al., 1985a; Jury *et* al., 1985b; Jury, 1987). Areas of wind shadow were also observed in these case studies stretching north-westward off the northern portion of the peninsula. Here warmer waters were found to correspond with decreased wind speed as a result of orographic obstruction (Jury, 1985; Jury *et* al., 1985a; Jury *et* al., 1985b; Jury, 1987). Figure 2.6 shows three case studies during November 1979 of wind flow and SST data from 150 m aerial surveys taken from Jury *et al.*, (1985b). During the SE winds, an upwelling plume and strong temperature gradients can be seen west of the Cape Peninsula, whereas SW winds result in the weakening of this upwelling plume as warmer waters move shoreward (Jury *et al.*, 1985b).

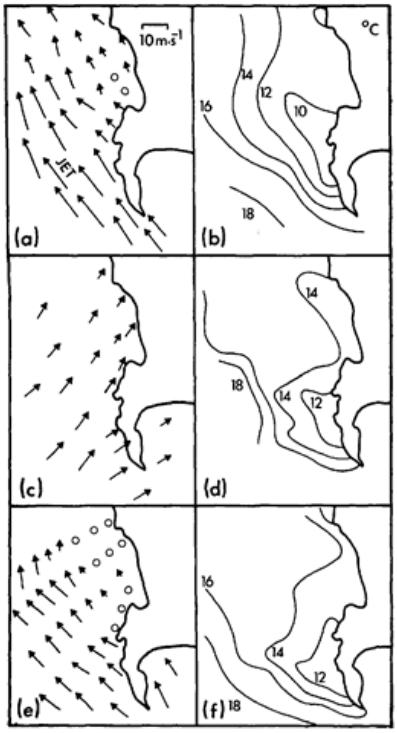


Figure 2.6. Wind (a, c, e) and sea surface temperature (b, d, f) derived from aerial surveys . The length and orientation of the arrows depicts wind speed strength and wind direction in a, c and e. Thermal fronts are shown in b, d and f. Three case studies are shown, one for a south-easterly winds on 18 November 1979 (a & b), another for a south-westerly wind on 20 November (c & d) and again a south-easterly wind on 22 November (e & f). From Jury *et al.* (1985b).

These upwelling plumes have also been observed in satellite imagery (Shannon *et al.*, 1983; Lutjeharms *et al.*, 1991; Shannon *et al.* 1991). Lutjeharms *et al.* (1991) used high-resolution infrared satellite data spanning 3 years to identify five frequently occurring frontal patterns within the bay and linked these to the wind regime. The first pattern was an upwelling plume off Cape Hangklip observed during predominantly SE winds. The second pattern was observed during strong and enduring south-easterlies with the same upwelling plume but with filaments spreading north-westward into the bay. Thirdly, a temperature front located across the mouth of the bay with cooler water within the bay was seen during persistent SE winds. Fourthly, a similar front found 40 km south of the mouth was seen during predominantly SE winds but with more NW winds than the previous feature. Finally, a front within the bay itself was observed with colder water on the east and warmer waters along the western shores which persisted for up to four days. This was observed during months when winds blew from various directions, but SE winds were slightly more frequent. Of these features, this front within the bay was the least frequent and the front 40 km south of the mouth was the most frequent. The predominant wind regime of each frontal feature was determined by comparing the wind roses for the individual calendar month in which the frontal feature had the highest occurrence and the same month within the three-year period in which it occurred the least. It must be noted that the

conclusion of Lutjeharms *et al.* (1991) were largely based upon a qualitative interpretation of the SST imagery.

A more recent study by Dufois & Rouault (2012) used 11 years of MODIS data to explore the interannual variability of SST in False Bay. They showed more variability in the northern half of the bay explained by seasonality whereas the southern half of the bay was largely influenced by the west coast upwelling processes rather than seasonality.

2.4.3. Ocean colour

2.4.3.1. Colour fronts

In addition to thermal fronts, distinct colour fronts can also be found in False Bay. These fronts are prominent in the northern region and are visible in satellite imagery and even to the naked eye as milky-green water seen closer to the shore and dark-blue clear water seen further into the bay (Shannon *et al*., 1991). Suggestions have been made on what causes these colour fronts, with studies showing that they are not the result of pollution (Shannon *et al*., 1982; Shannon *et al.*, 1991). Compositional studies of the milky and darker waters showed that the predominant difference between the fronts was in the abundance of biota, but not in the algal or faunal assemblages (Shannon *et al.*, 1991). A cross frontal study was performed by Waldron *et al*. (2008) comparing several different factors between the milky-green and blue-green waters. The milky waters were found to be warmer, richer in nitrate, silicate and calcium and contain more Chl-a, whereas the blue-green waters were richer in silicon. Although both waters were similar in their weights of suspended materials, those of milky-green waters were more abundant and fragmented and these waters were more turbid (Waldron *et al*.,2008). These fronts are not the result of algal blooms as not enough nutrients have been found in the milky-green waters to cause such a front (Shannon *et al*., 1991). Waldron *et al*. (2008) suggest that the milky colour of the coastal front may be due to strong southerly onshore winds bringing calcium and other sediment up from the sea bed into the water column as well as introduction from the land-sea interface.

Remote sensing has been used to observe these colour fronts. Using satellite imagery, four distinct categories of frontal features were identified along the northern shore of the bay and linked to the prevailing wind regime (Shannon *et al*., 1991). The first front was described in the north eastern corner and Gordon's Bay, the second at the near-shore zone at the north of the bay between Eersteriver and Strandfontein, the third was found in the north-western corner and Muizenberg and the fourth was a tongue-like feature located offshore of the northern shore (Fig. 2.7). An analysis of the predominant wind regimes present when these features occurred showed that the first feature occurred predominantly in winter during lighter westerly winds, the second was associated with moderate variable winds and the third and fourth occurred mostly in summer with strong SE winds. These frontal features have been compared to thermal satellite images, however, little coherence between

thermal structure and Chl-a was found, although upwelling was evident off Cape Hangklip and warmer waters were often observed along the north east corner of the bay (Shannon *et al*., 1991).


Figure 2.7. A map of False Bay. A) Muizenberg, B) Strandfontein, C) Eersterivier, D) Gordon's Bay. Source: ESRI_Imagery_World_2D

2.4.3.2. Harmful Algal Blooms (HABs)

Harmful Algal Blooms are algal blooms that can cause anoxic conditions and potential death of marine life (Pitcher *et al.*, 2008). Upwelling systems are susceptible to HABs due to their productive nature and HAB events have been described in upwelling systems all over the world, as discussed in a review by Pitcher *et al*. (2010). Several factors influence the formation of HABs, one of these being wind stress as this determines the amount of upwelling that occurs (Pitcher *et al*., 2010). Winds also influence circulation patterns, which can help introduce HABs into different areas or create retention zones were blooms can accumulate (Pitcher *et al*., 2010). False Bay is recognised as an area of elevated phytoplankton biomass and is at risk of experiencing HABs (Pitcher *et al*., 2010). Previous HABs have been recorded in the bay (Horstman *et al*., 1991; Pitcher & Calder, 2000), such as the red tide that occurred in 2007 (Pitcher *et al.*, 2008). Blooms are often concentrated in the north-eastern corner of the bay, possibly due to the presence of a circulation cell near Gordon's Bay (Pitcher *et al.*, 2008; Jacobson *et al*., 2014). To the east of the bay lies an upwelling cell of the Agulhas Bank, and due to cyclonic circulation in the bay during summer months (Atkins, 1970a; Jacobson, 2014), nutrient rich water from this upwelling region can be brought into the bay. Upwelling also occurs within the bay, further increasing nutrient concentrations and a nutrient front has been detected off Cape Hangklip during strong SE winds (Taljaard, 1991). This increase in nutrient rich waters as well as warmer summer waters, stratification during summer months and water residence time within the bay can

create a favourable environment for the possible formation of HABs (Pitcher *et al.*, 2008; Pitcher *et al*., 2010).

## 2.5. High resolution satellite derived wind data

### 2.5.1. Synthetic Aperture Radar (SAR)

Synthetic Aperture Radar (SAR) satellites can be used to better understand ocean and atmosphere dynamics as they provide information on a wide range of processes including air-sea interactions and ocean-atmosphere dynamics (Monaldo & Beal, 2004), surface winds, ocean surface currents, surface waves, internal waves, shoals, sea ice and rainfall (McCandles & Jackson, 2004). SAR are active radar satellites, meaning they transmit their own signal and then measure the backscatter from the return signal. The amount of backscatter depends on ocean surface roughness or Bragg waves, which are small wind-generated waves that are of a similar wavelength to that of the radar (Holt, 2004; McCandles & Jackson, 2004). The rougher the ocean surface, the greater the backscatter (Monaldo & Beal, 2004). The microwave signals are either vertically (V) or horizontally (H) polarized and polarisation can differ for transmission and retrieval. This results in co-polarised images (HH or VV) or cross-polarised images (HV or VH). The backscatter signals are then normalised to form Normalised Radar Cross Sections (NRCS) images (Dagestad *et al*., 2013). From these NRCS, wind speed can then be derived using various models. Winds speeds derived from SAR imagery have spatial resolution of typically 500 m to 1000 m allowing for the analysis of sub-mesoscale processes that cannot be resolved by scatterometers of poorer resolution (25-50 km) (Dagestad *et al*., 2013). SAR as well suited to the observation of winds in coastal areas, as data are available all the way to the coastline at a high resolution in contrast to scatterometers for which land contamination and low spatial resolution (25 km) result in missing data near the coast. Another advantage of SAR is its use of microwave frequencies which can go through clouds, unlike high resolution satellite data for SST and chlorophyll which use passive sensing of the visible and infrared spectrum that cannot penetrate clouds. In addition to this, SAR images can also be taken both day and night as they are not dependant on solar illumination (Holt, 2004).

One of the drawbacks of SAR derived winds is that wind direction cannot be directly observed and must be taken from other resources. Wind streaks seen in the images can provide some indication of wind direction, however with 180 ° ambiguity (Dagestad *et al*., 2013).

SAR imagery has mostly had a low temporal resolution and global coverage in part due to their high energy requirements in comparison to scatterometers. Additionally, SAR data has mostly been proprietary and is not always available for academic research, making the acquisition of high-resolution data for coastal studies more challenging. The Sentinel-1 mission is changing this with satellites providing images of the entire Earth every six days (www.esa.int/Our_Activities/Observing_the_Earth/Copernicus/Sentinel-1/Introducing_Sentinel-1).

This increase in SAR coverage and now freely available data present a new and exciting opportunity to improve our understanding of coastal winds.

### 2.5.2. Applications of SAR

Since the first SAR satellite, SEASAT, was launched in 1987 (Dagestad *et al.*, 2013), many studies have been performed using SAR on different aspects of physical oceanography, including surface winds (Vachon *et al*., 1998; Horstmann *et al*., 2000; Hasagar *et al*., 2005; Krug *et al*., 2018), ocean circulation (Rouault *et al*., 2010; Danilo *et al*., 2007; Qazi *et al*., 2014) and internal waves (Hsu *et al*., 2000; Liu & Hsu, 2004; Li *et al*., 2008). Horstmann *et al.* (2000) characterized the mesoscale wind field around the south of Greenland using RADARSAT-1 SAR data with C-band and HH-polarization. High resolution maps of wind speed were created for the Gulf of Alaska, Bering Sea and East Coast of United States using SAR imagery with average wind estimates corresponding to wind speed data from buoys in these regions (Hasagar *et al*., 2005). Another study by Vachon *et* al. (1998) explored the spatial structure and wind field of intensive mesoscale cyclones over the Labrador Sea using SAR imagery from the RADARSAT and ERS satellites. A study by Krug *et al*. (2018) explored the signature of the Agulhas Current on high resolution satellite derived wind speeds using Advanced Synthetic Aperture Radar (ASAR) data along with altimeter data. The study found that both SST and the direction of ocean current relative to the wind influenced these satellite derived winds.

An important application of SAR is its ability to capture winds speed estimates in coastal regions due to its high spatial resolution. This was demonstrated by the Alaska SAR Facility in the Alaska SAR Demonstration where SAR data were used to obtain high resolution wind speed in coastal areas, with features such as wind jets and wind shadows created by the coastal topography detectable in these images (Monaldo, 2000) (Fig. 2.8). This ability for SAR data to capture coastal wind fields was again shown in another study by Monaldo *et al*. (2001) in which SAR wind speed estimates were compared with buoy measurements and model predictions, with a high agreement being found. Other studies have also demonstrated the ability of SAR data to capture fine scale variability in the wind field and orographic effects in coastal regions, such as a global study using ERS-2 satellite SAR data by Lehner *et al. (*2000) and a study along the Norwegian coastline by Korsbakken *et al*. (1998).

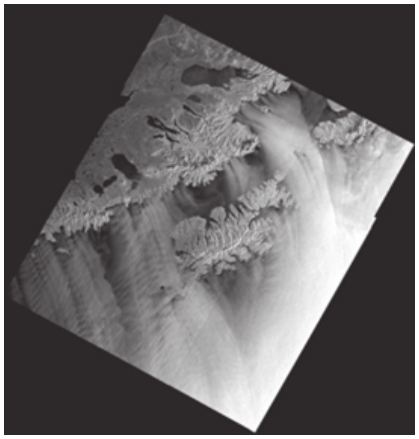

Figure 2.8. A SAR image near Cook Inlet and Kodiak Island off Alaska, taken during the Alaska SAR Demonstration and processed by the Alaska SAR Facility. Wind accelerations and wind shadows can be seen in lee of the coast. From Monaldo (2000).

### 2.5.3. Wind and high-resolution SST and chlorophyll

Unlike wind data, high-resolution SST and chlorophyll data have often been used in coastal studies, with data at 1 km resolution being freely and routinely available for more than twenty years. Current satellites providing these products include the NOAA Suomi National Polar-orbiting Partnership (SNPP) with the VIIRS sensor, the NASA Aqua satellite with the MODIS sensor, as well as the EUMETSAT Sentinel-3 satellites with OLCI (Chl-a) and SLSTR (SST) sensors. A study by Weeks *et al*. (2006) provides an example of such data being used to explore variability near the coast. Weeks *et al*. (2006) used five years of high resolution (1 km) satellite imagery for SST and chlorophyll to explore variability in upwelling and phytoplankton response within the Southern Benguela. Other studies using high-resolution satellite data to explore SST and Chl-a include DiMarco *et al.* (2000), Kuo *et al.* (2000), Demarcq *et al.* (2003) and Dufois & Rouault (2012) to name a few. These high-resolution data have allowed for the exploration of variability in both temperature and the biology near the coast, but not necessarily in synergy with observations of the drivers of this variability. Some studies of this nature have been performed, for example, Gagliardini *et al*. (2000) used SAR imagery along with thermal infrared imagery to explore frontal features in the Brazil-Malvinas confluence during moderate wind conditions (less than 10 m/s) finding correspondence between frontal features in the infrared and SAR images. Additionally, the higher resolution of the SAR images allowed for the detection of finer scale frontal features (Gagliardini *et al*., 2000).

Despite the potentials of SAR data, it has not yet been used to describe coastal wind speeds along the coast of South Africa. In this study, the use of high-resolution SAR wind estimates in synergy with high resolution SST and chlorophyll data is explored. This high-resolution wind data will be used to better understand the wind variability in False Bay and the surrounding coastline, and ultimately to help us better understand the impact of wind forcing on the other physical aspects within the bay.

## 3. METHODS

The study region lies between longitudes 18 and 19 ˚E and latitudes 33.5 and 34.5 ˚S and includes both False Bay and the Cape Peninsula. False Bay is defined as the area between Cape Point and Cape Hangklip and the Cape Peninsula is defined as the region stretching from Cape Point to Table Bay (Fig. 2.1).

### 3.1. Data

#### 3.1.1. Ocean winds

In order to explore variability in the wind field of False Bay and the Cape Peninsula, both measured and modelled wind speeds were analyzed.

##### 3.1.1.1. SAR derived wind speeds

Synthetic Aperture Radar (SAR) data of Interferometric Wide (IW) swath mode resolution, obtained by the Sentinel-1 satellite for the European Space Agency (ESA) mission, was used to produce high resolution ocean surface winds within False Bay and the Cape Peninsula. Compared to other methods such as ScanSAR, IW mode and TOPSAR decreases scalloping effects on the image as well as noise (Sentinel-1 SAR User Guide, ESA). SAR produces Normalised Radar Cross Sections, or NRCS images from which wind speed is then derived.

For this study, vertically co-polarised (VV) NRCS images and the GMF CMOD5.N were used to derive wind speed. GMFs relate surface roughness to wind speed and CMOD5.N is tuned for winds at 10 m above the ocean's surface (Takeyama *et al*., 2013). CMOD5.N has been shown to be the optimum GMF to derive winds in coastal regions (Takeyama *et al*., 2013). Using aircraft measurements and *in situ* wind speed observations, CMOD5 has been tuned to 22 million ERS-2 NRCS and ECMWF wind collocations (Dagestad *et al*., 2013). This has allowed for better derived higher wind speeds and a decrease in incidence angle biases from previous versions. CMOD5.N is an updated version of CMOD5 and avoids atmospheric stratification errors by producing 10 m winds for neutral conditions (Dagestad *et al*., 2013). Additionally, to compensate for average stability and a low bias, CMOD5.N adds 0.2 and 0.5 m/s to winds (Dagestad *et al*., 2013). CMOD5.N is a widely used GMF and can accurately derive wind speeds between 2 and 35 m/s (Takeyama *et al*., 2013). All SAR data was processed by IFREMER.

##### 3.1.1.2. ECMWF modelled winds

Modelled wind speeds for comparison with those derived from the SAR images were obtained from the European Centre for Medium-Range Weather Forecasts (ECMWF) models. Here, hourly ECMWF models wind speed and direction outputs generated at a spatial resolution of 9km were used. These zonal and meriodional winds were interpolated to a spatial resolution of 1 km using bilinear

interpolation. The resulting 1 km wind direction from the ECMWF modelled winds were used to derive SAR wind speeds.

3.1.2. SST and Chl-a

The variability in ocean surface temperatures and chlorophyll within False Bay were assessed with daily level 2 data products for SST and Chl-a. Subsets of these data products were obtained from the NASA Ocean Biology Processing Group website (https://oceancolor.gsfc.nasa.gov/) for the False Bay region for the period of January 2012 to the end of December 2017. These products were obtained for both the Visible and Infrared Imager/Radiometer Suite (VIIRS) instrument onboard the Suomi National Polar-orbiting Partnership (SNNP) satellite, as well as for the Moderate Resolution Imaging Spectroradiometer (MODIS) instrument onboard the Aqua satellite. The MODIS and VIIRS data have a spatial resolution of 1 km and 750 m, respectively. Chl-a was used as a proxy for phytoplankton biomass.

3.1.3. Bathymetry and elevation

GEBCO gridded bathymetry data (GEBCO_2014 Grid) was used to explore the bathymetry within the bay as well as the topography of the surrounding land. Bathymetry is shown in contours of -30 m, -50 m, -100 m, -200 m and -300 m to investigate ocean depth, and elevation up to 1000 m is shown using a colour bar to explore topographic features.

3.2. Methods

Within the year 2017, there were 13 days of SE winds where adequate SAR, SST and ocean color data were all available. Wind, SST and Chl-a variability was explored for all 13 cases. All analyses were performed using python scripts.

Several case studies were selected and are presented in this document to highlight common patterns observed, including orographic impacts in the wind field, SST variability and Chl-a. However, all figures and calculations were performed for each of the 13 days for 2017 and are presented in appendix A-J.

3.2.1. SAR wind, SST and Chl-a maps

SAR derived wind speed maps were created to visualize wind variability in False Bay and the Cape Peninsula area and ECMWF modelled wind directions were overlaid on these maps. Both VIIRS and MODIS SST and Chl-a maps were created for each day to visualize variability in temperature and biology within the study area. MODIS and VIIRS SST and Chl-a products were very similar. For this study, only VIIRS maps are presented as these data have a higher spatial resolution (750 m).

3.2.2. SAR vs modelled winds

The difference between SAR derived winds and ECMWF modelled wind speeds were also plotted in order to determine if high resolution global atmospheric models were able to capture the true variability in the wind regime. It is anticipated that most of the coastal variability linked to the orography will not be adequately captured in the ECMWF product. Should that be the case, maps of the wind speeds differences in between the SAR and ECMWF will allow us to characterise the spatial extent and as well as the magnitude of wind shadows and regions of localised enhanced winds.

### 3.2.3 Ekman pumping

For each case, wind stress was calculated using the drag coefficient of Yelland & Taylor (1996) and Ekman pumping was derived from the wind stress and plotted. Ekman pumping (ω) represents the vertical transport induced by the wind stress at the ocean's surface, where a negative value for Ekman pumping indicates upwelling, and a positive value indicates downwelling (Tomczak & Godfrey, 2013). The equation used to calculate Ekman pumping (ω) is presented below as Equation 1, where τ is the wind stress, $\tau_x$ and $\tau_y$ are the x and y components of τ and $f$ is the Coriolis force (Tomczak & Godfrey, 2013). A reference density ($\rho_0$) of 1025 kg/m3 was used.

Equation 1.

$$-\rho_0\omega = \text{curl}\,(\tau/f) = \partial(\tau_y/f)\,/\,\partial x - \partial(\tau_x/f)\,/\,\partial y$$

### 3.2.4. Transects

In order to explore co-variability in wind, SST and Chl-a, transects were selected across False Bay (-34.25 S, 18 E to -33.7925 S, 18.4575 E) and the northern portion of the Cape Peninsula (-34.3958 S, 18.5 E to -34.0833 S, 18.8125 E). The position of these transects is shown in Figure 3.1. These transects cross areas of False Bay and the Cape Peninsula where wind shadows occur and where high wind variability is observed during SE winds.

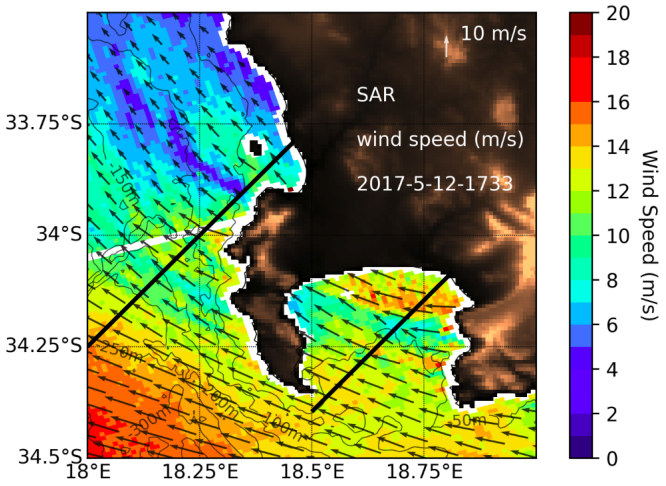


Figure 3.1. The position of two transects, one across False Bay and the other across the northern section of the Cape Peninsula, used to examine co-variability between wind speed, sea surface temperature and chlorophyll concentrations.

### 3.2.5. Time series

Regions of intensified or reduced winds were identified in False Bay and on the western side of the Cape Peninsula. These selected regions, or boxes, of strong spatial wind variability are defined in Table 3.1 and Figure 3.2. Monthly VIIRS SST and Chl-a were spatially averaged over these boxes and plotted in time series over the period 2012 to 2017. These were then compared to ERA-interim v-component wind speed values rotated along a north-west – south-east axis for a point offshore of False Bay (Table 3.1). ERA-interim wind speeds were obtained from the ECMWF website (https://www.ecmwf.int/en/forecasts/datasets/archive-datasets/reanalysis-datasets/era-interim) and have a spatial resolution of approximately 80 km and a temporal resolution of 6 h (Dee *et al.*, 2011). Winds in False Bay are predominantly aligned along a north-west to south-east axis, with SE winds being upwelling favourable. The rotation of the winds along a north-west to south-east axis was done to better highlight instances of upwelling favourable winds. Additionally, the difference between the wind shadow and upwelling boxes were calculated for both SST and ocean color and compared to the rotated winds to explore seasonality.

Table 3.1. Boxes highlighting the spatial extent of identified regions of stronger and weaker winds. Longitude and latitude are in decimal degrees.

| | North | South | East | West |
|---|---|---|---|---|
| False Bay upwelling | -34.305 | -34.405 | 18.675 | 18.825 |
| False Bay wind shadow | -34.155 | -34.255 | 18.685 | 18.835 |
| Cape Peninsula upwelling | -34 | -34.15 | 18.25 | 18.35 |
| Cape Peninsula wind shadow | -33.805 | -33.995 | 18.275 | 18.375 |
| ERA-interim v-component wind speed | | -34.5 | | 18.75 |

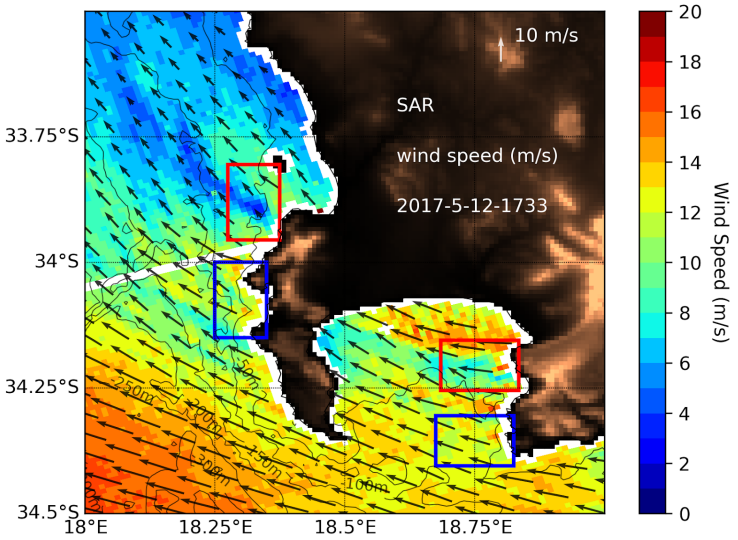


Figure 3.2. SAR wind speed (m/s) on 12/05/2017 with wind vectors overlaid.The position of the boxes used to calculate monthly mean sea surface temperature and chlorophyll concentrations for areas of upwelling (blue) and wind shadow (red) in False Bay and off the Cape Peninsula are shown.

# 4. RESULTS

## 4.1. Wind variability over False Bay and the Cape Peninsula

Two case studies representative of a strong SE and weak SE wind regimes were selected from a total of 13 SAR images collected over the year 2017. The spatial variability in the wind fields during a strong SE (2017-05-12, Fig. 4.1A) and a weak SE (2017-10-22, Fig. 4.1B) is analysed. Please note that in Figure 4.1B, the Sentinel-1 swath only images the eastern part of the study region, resulting in no data west of the Cape Peninsula.

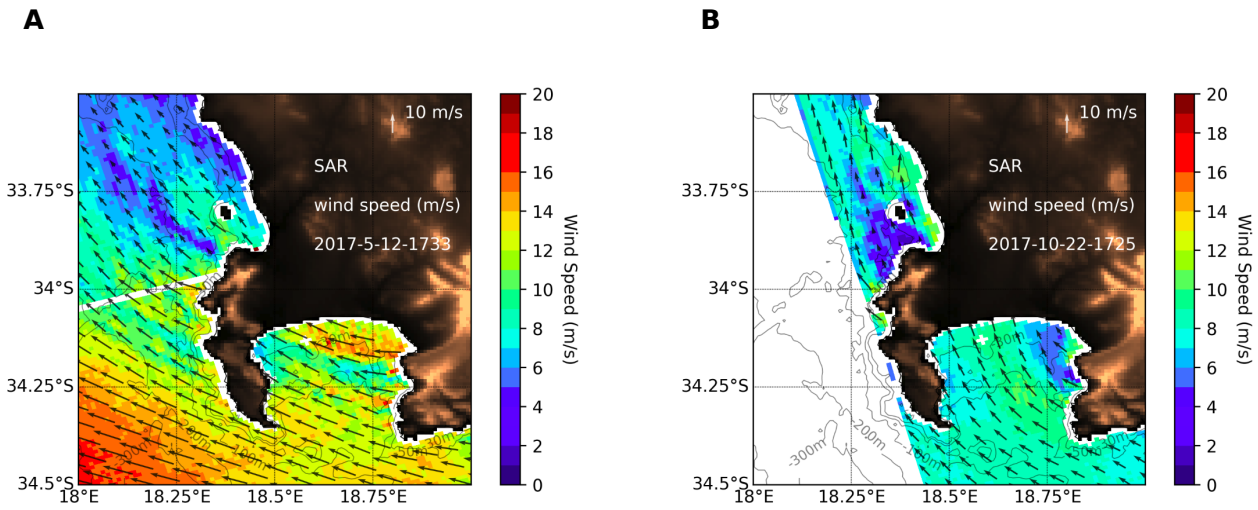


Figure 4.1. SAR derived wind speeds in m/s for a case of a strong south-easterly winds (A, 2017-05-12) and weak south-easterly winds (B, 2017-10-22) in False Bay and the Cape Peninsula. The length of the arrows depicts SAR derived wind speeds and wind direction was taken from ECMWF modelled winds.

### 4.1.1. SAR derived wind estimates

Spatial variability was evident in the SAR derived wind speed maps. Winds for the strong SE case ranged from 3.3 m/s to 19.7 m/s (Fig. 4.1A) and from 1.4 m/s to 11.7 m/s for the weak SE case (Fig. 4.1B). The background wind speed for the strong and weak case was 11.5 m/s and 8.0 m/s, respectively. The strong SE case showed a larger range of wind speed, however, it is difficult to compare the two cases in terms of maxima and minima as the area of maximum wind speed in the weak SE case may fall offshore of the Cape Peninsula where no data was available. High wind variability is still very notable across the wind shadow zone off of Cape Peninsula for both cases, and on average stronger winds can be seen within False Bay (Fig 4.1).

Within False Bay, a wind shadow was seen spreading west-northwestward into the bay, stretching right across the entire bay during stronger winds covering a distance of about 41 km in length and 8

km in width. This wind shadow occured in lee of the highest mountain ridge of the Cape Hangklip mountain range. The orientation of this wind shadow changes depending on the direction of the wind, but it should be noted that the wind direction during the stronger SE case (Fig. 4.1A) is more representative of typical SE conditions (Appendix A). The wind direction differs between the strong (Fig. 4.1A) and the weak (Fig. 4.1B) cases of SE winds, with the former showing a more south-east direction and the latter showing a more south-southeast direction. This seems to affect the position of the wind shadow within False Bay and north of the Cape Peninsula, with the weaker case showing a wind wake coming from a more southerly direction in comparison to the strong SE case (Fig. 4.1). For the strong south-easter case, wind speed within the wind shadow area of False Bay was approximately 8 m/s, with adjacent areas of wind acceleration having winds as strong as 15 m/s (Fig. 4.1A). For the weaker case, winds as low as 4 m/s were seen in the wind shadow, and wind increases of up to 9 m/s can be seen on either side (Fig. 4.1B).

A prominent wind shadow was also seen in lee of the northern portion of the Cape Peninsula mountains, stretching northwestward away from the peninsula for both cases (Fig. 4.1). This wind shadow was approximately 32 km in length and as wide as 16 km for the weak wind case and 34 km long and 7 km wide for the strong wind case. The wind shadow off the Cape Peninsula stretched as far as 62 km in some of the case studies (Appendix A). This decrease in winds relative to the background wind was greater than that in False Bay, with winds as low as low as 4 m/s being found during both the strong and weak SE winds (Fig. 4.1). Overall, stronger winds were present within False Bay itself in comparison to the region north of the Cape Peninsula (Fig. 4.1A). Wind acceleration was observed off Cape Hangklip and Cape Point, with lines of wind acceleration and less prominent wind shadows along the southern portion of the Cape Peninsula caused by the mountain ridges. Additionally, wind speeds tended to increase as one moves further offshore from the continent. These areas of wind shadow and acceleration are most likely the result of a capping inversion layer and vertical compression resulting from the southward ridging of the SAA as suggested in previous studies (Atkins, 1970b; Van Foreest & Jury, 1985; Jury, 1987; Jury, 1991)

4.1.2. Measured vs modelled wind speeds

Much less spatial variability was observed in the ECMWF modelled wind speed maps over the entire study region. These maps can be seen in Appendix B. Large differences between the SAR and ECMWF wind speeds were observed for both the strong (Fig. 4.2A) and weak (Fig. 4.2B) cases of SE winds, with differences ranging from 0 m/s to 12.9 m/s and 0 m/s to 7 m/s, respectively. These differences between the SAR and the modelled wind speeds essentially highlight regions of high spatial variability near the coast which cannot be captured in the global numerical model. In Figure 4.2, the spatial extent of wind shadows and regions of intensified wind is clearly visible. During the strong SE winds experienced on 12 May 2017 (Fig. 4.2A), SAR wind speeds were as high 10 m/s greater than those predicted by ECMWF over most of False Bay, with the exception of a narrow region in the

middle of the bay, where SAR wind speeds were about 1 to 2m/s below the ECMWF wind speeds. This region where ECMWF overestimates wind speeds corresponds to the area of wind shadow shown in the SAR image for this case (Fig. 4.1A). A similar pattern was seen in the weak SE case, where areas of decreased winds and wind acceleration seen in Figure 4.1B correspond to areas where the ECMWF model under predicts and over predicts winds in Figure 4.2B. For this case the greatest difference lies in the wind shadow off the Cape Peninsula with ECMWF wind being up to 7 m/s greater than the SAR winds (Fig 5.2B). Additionally, ECMWF model tended to predict a wind shadow along the north-east coast of False Bay which is in disagreement to the SAR imagery and results in large differences in wind speed as seen in Figure 4.2.

The main outcome from these figures was that high-resolution global atmospheric models, such as ECMWF, does not capture the full spatial variability in these coastal regions, with areas of most difference corresponding to areas affected by orographic effects. These differences were as large as 7 m/s greater or 12 m/s lower than the measured wind speeds (Fig. 4.2). The majority of these differences occur in areas largely affected by the surrounding coastal topography, where winds in lee of coastal mountains are prevented from flowing over very high mountain ridges forming wind shadows or are vertically compressed to create wind acceleration. This change from decreased to increased winds was very rapid and can occur over a short distance of less than 5 km. Although ECMWF does tend to simulate some orographic effect, the location of the wind shadow in lee of the Hottentot mountain range was incorrect. Here, a decrease in wind speed was predicted closer to the northern shore rather than in the middle of the bay as was seen in SAR images. ECMWF models produce winds of very high spatial resolution of 9 km, however, even with this high-resolution these models were still unable to capture the effect of land on coastal winds.

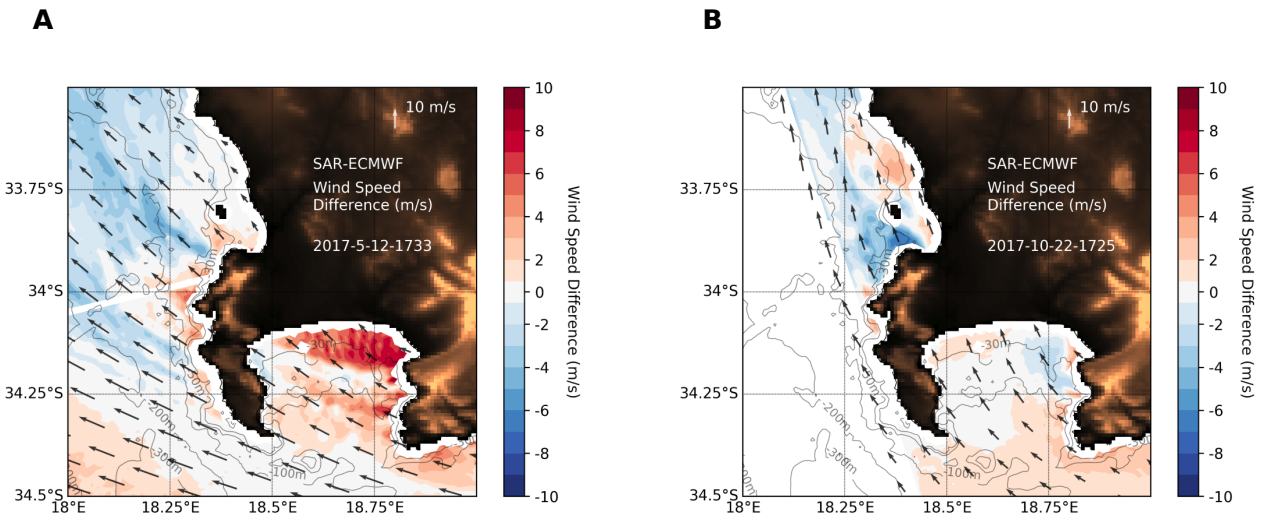


Figure 4.2. The difference between SAR derived wind speeds and ECMWF modelled wind speed in m/s for a case of strong south-easterly winds (A, 2017-05-12) and a case of weak south-easterly winds (B, 2017-10-22). The length of the

arrows depicts SAR derived wind speeds and direction was taken from ECMWF modelled winds. Red areas depict where SAR wind speed estimates are greater than modelled wind speeds and blue areas depict where winds are stronger in the model.

### 4.1.3. Ekman pumping

The strong spatial variability observed in the previous section over the Cape Peninsula and False Bay is expected to strongly impact the oceanic environment. Here, maps of wind stress curl were used in an attempt to characterise the impact of wind driven variability on convergence (front formation), retention, upwelling and downwelling.

SE winds in False Bay would cause an Ekman transport away from the coastline as the Coriolis force is directed to the left of the wind direction in the southern hemisphere. The magnitude of the Ekman transport increases with wind speeds. Spatial variations in the Ekman transport can create zones of flow convergence or divergence within the bay. Ekman pumping, which represents the horizontal divergence of the Ekman transport, is used here to highlight the impact of the ocean surface winds spatial variability on the circulation within the bay. Positive Ekman pumping values are associated with upwelling (divergence) while negative Ekman pumping values are associated with downwelling (convergence). Positive and negative Ekman pumping were seen within False Bay and off the Cape Peninsula. Positive Ekman pumping of up to 134.1 m/day and negative Ekman pumping of up to 180.3 m/day occurred during the strong SE case. Intense winds near the northern coastline of False Bay (Fig. 4.1A) were associated with a strong offshore Ekman flow and strong upwelling (as shown in Figure 4.3A). As the upwelled water was advected seawards away from the coast, it encountered a region of weaker winds and therefore weaker offshore Ekman flow. The coastal water was therefore slowed down in its seaward progress as it neared the wind shadow region and downwelling occurred. This resulted in an area of convergence across the bay. This area of convergence could result in the retention of waters in the northern half of the bay during strong SE winds. During weak SE winds, the magnitude of the upwelling and downwelling decreased but the same patterns of divergence and convergence were observed, with coastal waters similarly trapped in the northern section of False Bay (Fig. 4.3B). Such intense upwelling and downwelling cells are expected to lead to strong vertical mixing within the bay. For the Cape Peninsula, parallel streaks of upwelling and downwelling could be seen along its western shores during strong winds (Fig. 4.3A).

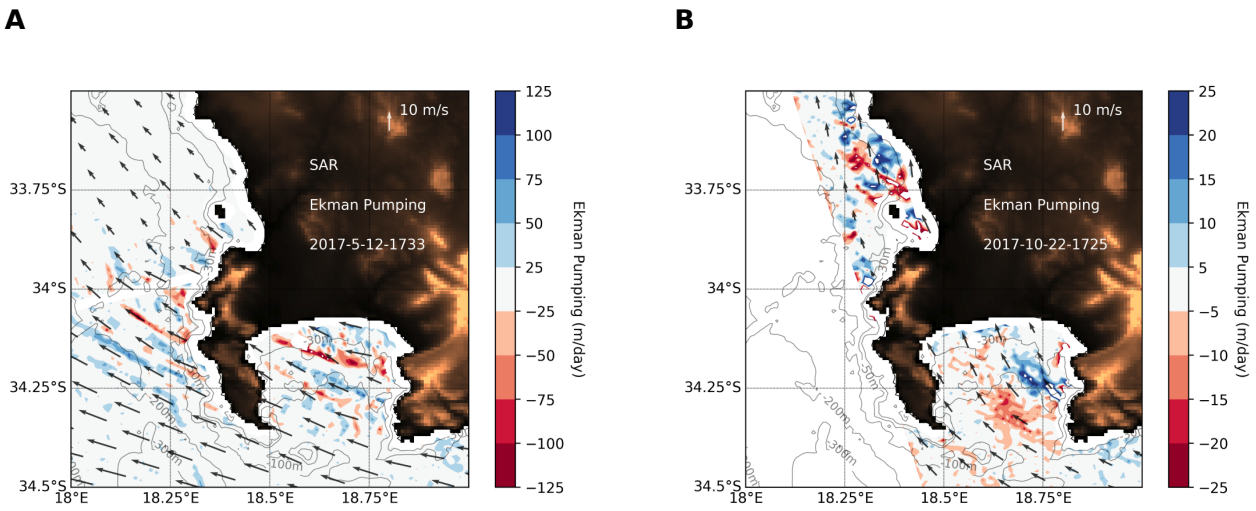


Figure 4.3. Ekman pumping maps in m/day over False Bay and the Cape Peninsula for a case of A) strong south-easterly winds (2017-05-12) and B) weak south-easterly winds. Arrow length indicates SAR derived wind speed in m/s and arrow direction indicates ECMWF modelled wind direction.

## 4.2. Co-variability in wind forcing, SST and Chl-a

### 4.2.1. SST and Chl-a during the selected case studies

SST and Chl-a observations collected at times of Sentinel-1 SAR acquisition showed a direct impact of the coastal varying winds on the ocean's surface properties. Variability in ocean surface temperatures for the case of intense winds ranged from 10.6 ˚C to 16.4 ˚C with an average temperature of 13.6 ˚C for the entire study region (Fig. 4.4A). For the case of weaker winds there was a background temperature of 16.2 ˚C with a SST range of 12.5 ˚C to 18.8 ˚C (Fig. 4.4B). It should be noted that these case studies are taken during two different seasons and this could affect the range in temperatures seen in the Cape Peninsula and False Bay region. Warmer SST was observed in wind shadow areas, and this was especially evident in the wind shadow off the Cape Peninsula with temperatures of about 15 ˚C observed in comparison to cooler waters of up to 11 ˚C seen in upwelling regions (Fig. 4.4A). These areas of upwelling depicted by colder SST could also be seen off Cape Hangklip and along the west coast corresponding to areas of increased winds (Fig. 4.1 and Fig. 4.4). A large upwelling cell was seen off the west of the Cape Peninsula with SST as low as 10.6 ˚C observed during stronger winds (Fig. 4.4A); the shelf in this region is very steep allowing upwelling of deeper and colder waters compared to False Bay. For False Bay, waters tended to be warmer in the northern section of the bay and cooler towards the mouth of the bay (Fig. 4.4, Appendix E). Further offshore from the continent, SST increased in most cases (Fig. 4.4). This increase in temperature seems to correspond to an increase in wind speed (Fig. 4.1).

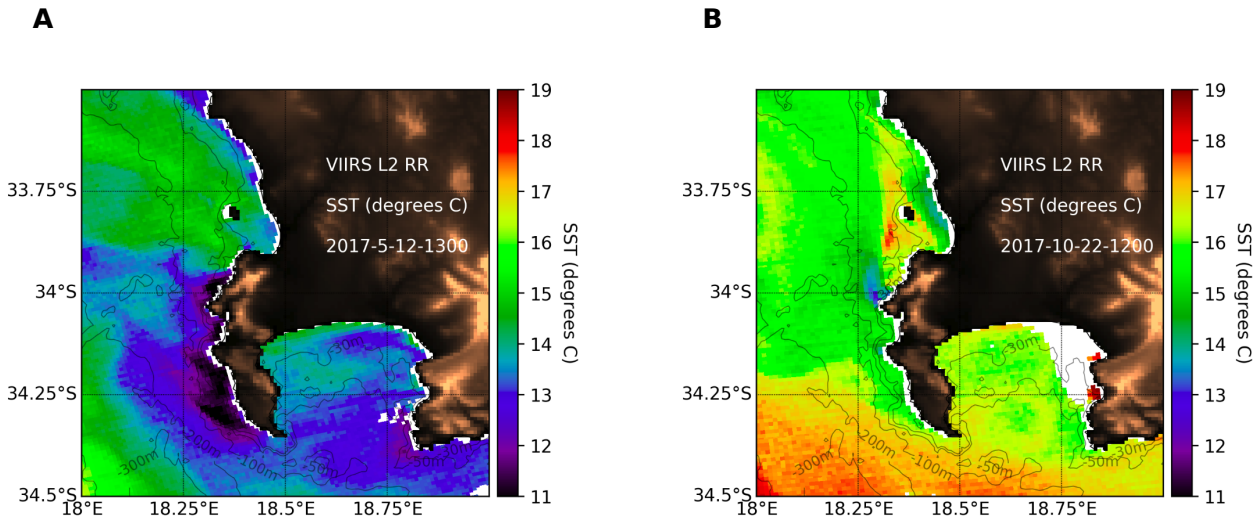


Figure 4.4. VIIRS sea surface temperature (SST) maps in degrees Celsius (degrees C) for a case of strong south-easterly winds (A, 2017-05-12) and a case of weak south-easterly winds (B, 2017-10-22) in False Bay and the Cape Peninsula.

In terms of Chl-a, no consistent patterns were found, however, within False Bay Chl-a seemed to be the highest along the northern shores with Chl-a of about 20 mg/m$_3$ compared to concentrations of between 1 to 3 mg/m$_3$ found at the mouth of the bay for the case studies presented here (Fig. 4.5). The main observation evident in many cases was that chlorophyll concentrations were not highest directly in the upwelling zones but rather further offshore in the retention zones. This can be seen in Figure 4.5A.

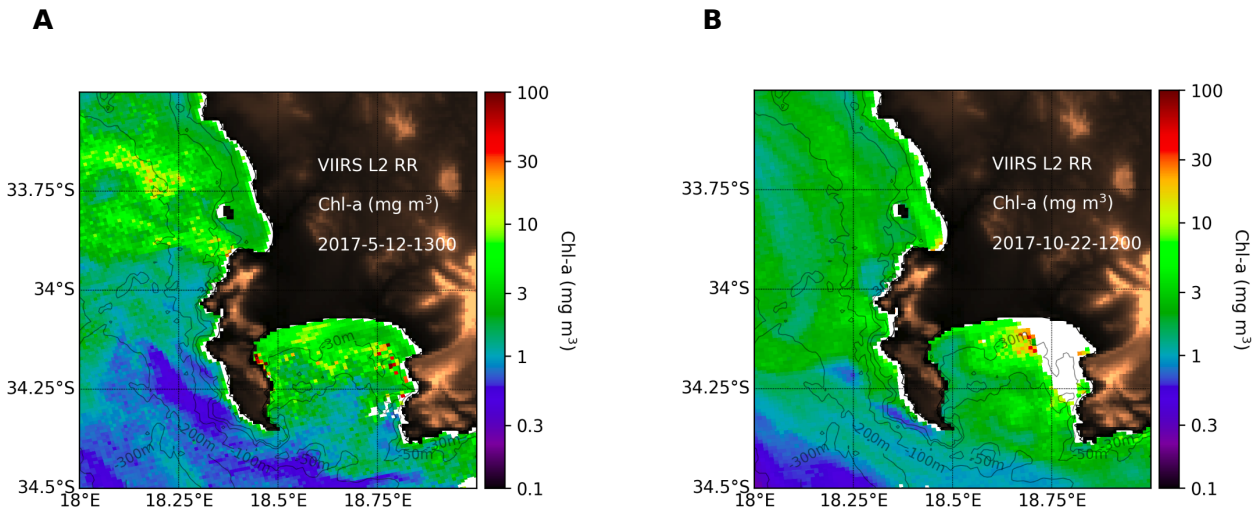


Figure 4.5. VIIRS chlorophyll concentration (Chl-a) maps in mg/m3 for a case of strong south-easterly winds (A, 2017-05-12) and a case of weak south-easterly winds (B, 2017-10-22) in False Bay and the Cape Peninsula.

Co-variability was most detectable between wind speed and SST (Fig. 4.6). Figure 4.6 shows a correspondence between a decrease in wind speed and an increase in surface temperature within the wind shadow area. This was most evident for the wind shadow zone off the Cape Peninsula where a decrease in winds to about 4.5 m/s coincides with an increase in SST peaking at about 15 ˚C for the strong wind case (Fig. 4.6C) and a low of 1.3 m/s coinciding with a peak of about 17 ˚C for the weaker wind case (Fig. 4.6D). Further offshore of the continent the coastal upwelling signature was no longer visible at the surface and higher wind speeds were observed together with higher ocean temperatures (Fig. 4.6).

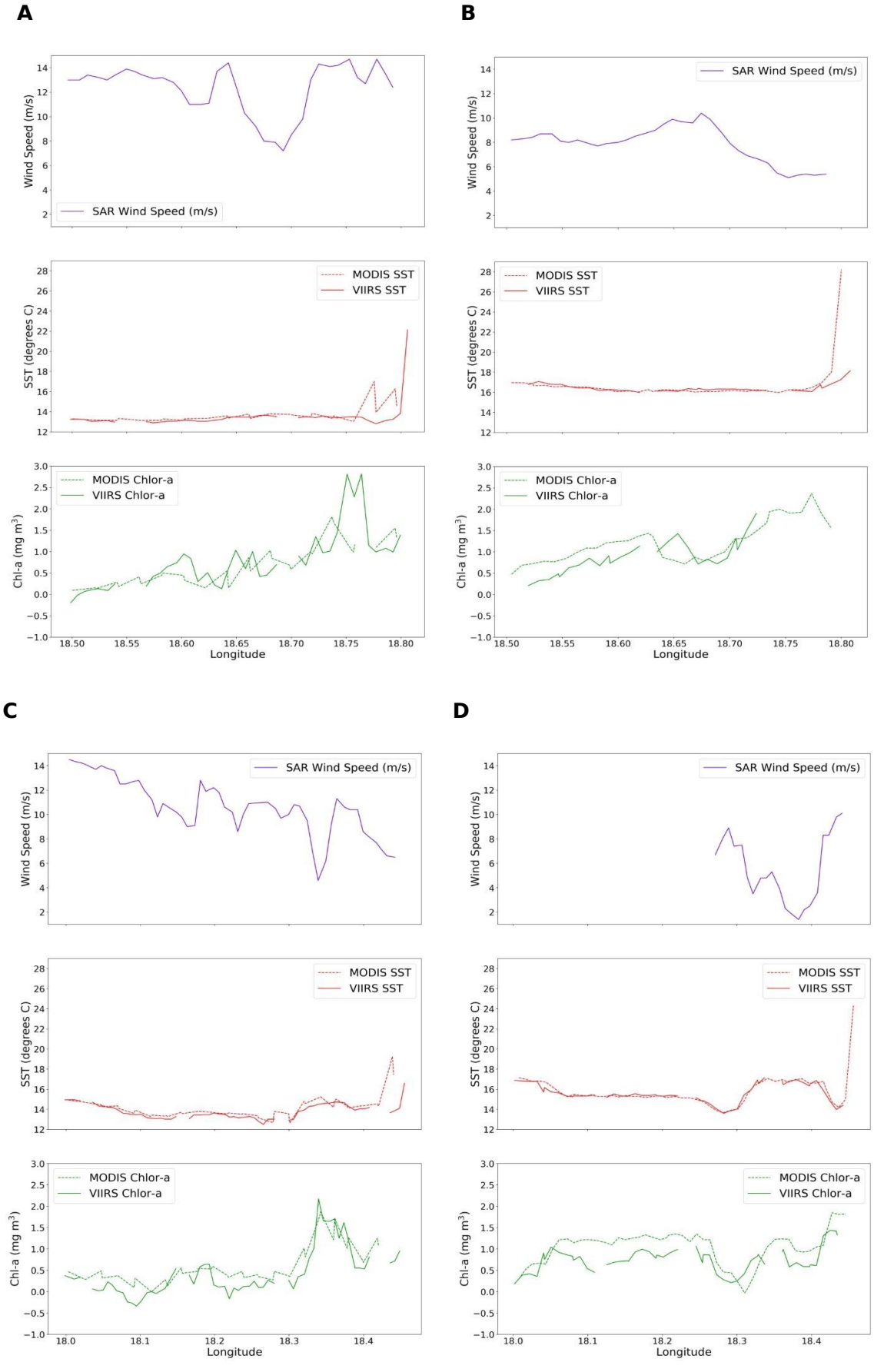
A
B
C
D
Wind Speed (m/s)
SAR Wind Speed (m/s)
SST (degrees C)
MODIS SST
VIIRS SST
Chl-a (mg m$^3$)
MODIS Chlor-a
VIIRS Chlor-a
Longitude

Figure 4.6. SAR derived wind speed (blue) as well as MODIS (dashed) and VIIRS (solid) sea surface temperature (SST) (red) and chlorophyll concentration (green) along a transect in False Bay (A & B) and off the northern section of the Cape Peninsula (C & D). Two case studies are presented, one for a case of strong south-easterly winds (2017-05-12, A & C) and another of weak south-easterly winds (2017-10-22, B & D).

### 4.2.2. Seasonality

A seasonal pattern was seen in the wind data, with predominantly SE winds during summer months, and an increase in NW winds during winter months (Fig. 4.7A). Strong seasonal variations were also observed in the SST and Chl-a datasets. A cyclical pattern was seen within the SST, with peaks during summer months and troughs during winter months (Fig. 4.7B). SST in the upwelling regions ranged from 13.4 ˚C to 19.0 ˚C and 11.7 ˚C to 15.8 ˚C for False Bay and Cape Peninsula, respectively. SST in the wind shadow regions were more variable with a range of 13.6 ˚C to 20.7 ˚C and 12.8 ˚C to 18.4 ˚C for False Bay and the Cape Peninsula (Fig. 4.7B). Surface temperatures were warmer in wind shadow zones (16.8 ˚C for False Bay and 14.9 ˚C for Cape Peninsula) compared to the upwelling regions (16.0 ˚C for False Bay and 14.0 ˚C for Cape Peninsula) (Fig. 4.7B). Overall, SST in the False Bay zones were warmer by about ~2$_{o}$C compared to the temperatures off the Cape Peninsula (Fig. 4.7B). Chl-a also showed some seasonal pattern, with the highest concentrations observed in summer months and lowest concentrations in winter months (Fig. 4.7C). Average concentrations were higher in the wind shadow regions (5.6 mg/m$_{3}$ for False Bay and 4.3 mg/m$_{3}$ for Cape Peninsula) than in the upwelling regions (3.0 mg/m$_{3}$ for False Bay and 2.4 mg/m$_{3}$ for Cape Peninsula) (Fig. 4.7C).

For the difference between wind shadow and upwelling zones, seasonality was seen in both SST and Chl-a. The average difference between the two regions for SST was 1 .0 ˚C for the Cape Peninsula and 0.89 ˚C for False Bay. Differences were as high as 2.7 ˚C (Cape Peninsula) and 2.4 ˚C (False Bay) greater in the wind shadow regions (Fig. 4.8B). These differences were highest during summer months showing warmer SST in wind shadow zones when more frequently SE winds occurred. During winter months differences were much lower, with upwelling regions even reaching temperatures slightly warmer than the wind shadow regions (up to 0.26 ˚C for Cape Peninsula and 0.76 ˚C for False Bay) for 5 out of the 6 years observed (Fig. 4.8B). These peaks in temperatures in the upwelling zone corresponded with peaks in NW winds (Fig. 4.8). Although temperature ranges were greater in False Bay (5.6 ˚C in the upwelling region and 7.1 ˚C in the wind shadow region) than for the Cape Peninsula (4.1 ˚C in the upwelling region and 5.7 ˚C in the wind shadow region) the temperature differences between wind shadow and the upwelling zones for each site were similar (mean difference of 1.0 ˚C in Cape Peninsula and 0.89 ˚C for False Bay).

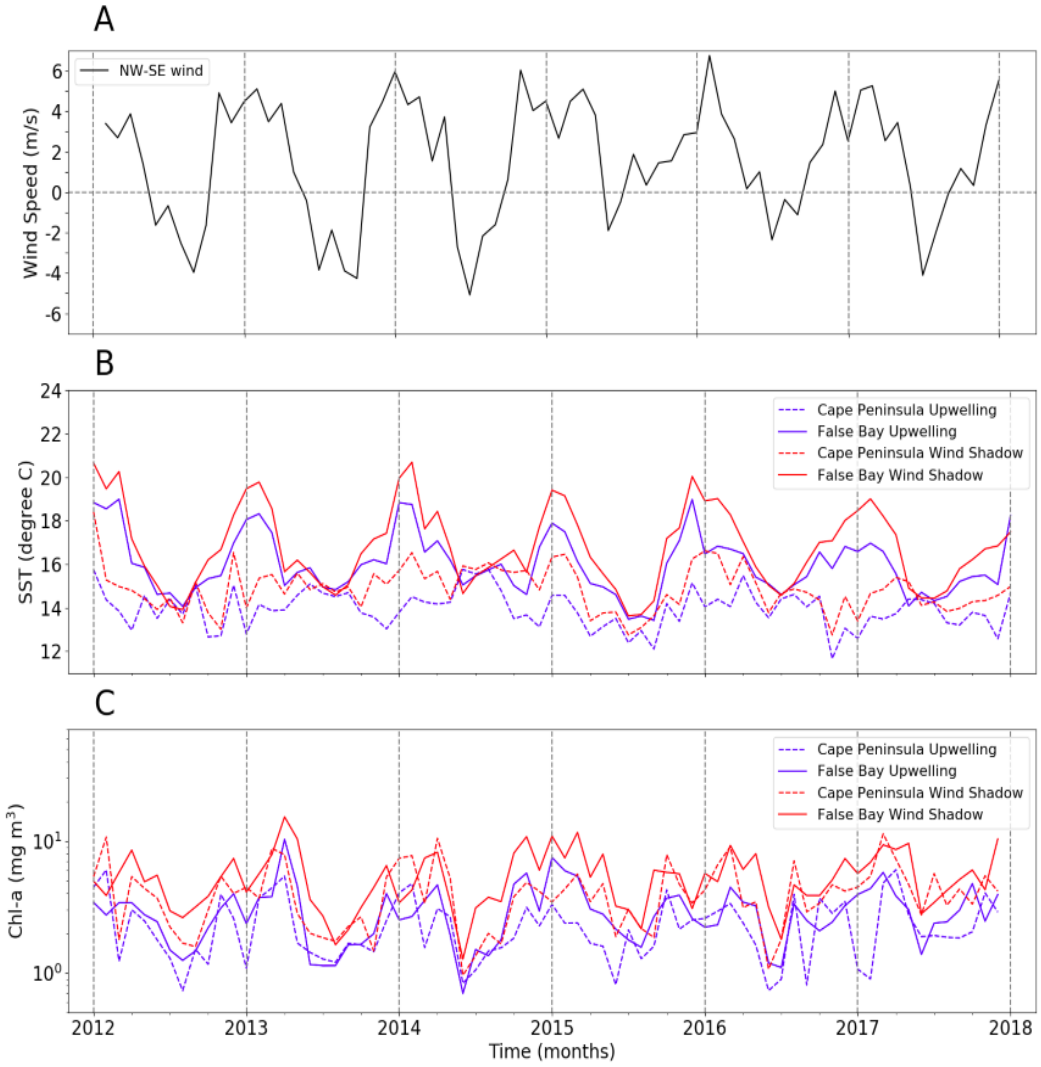


Figure 4.7. A time series of A) ERA-interim v-component wind speeds taken from a location off shore of False Bay (-34.5 S, 18.75 E) rotated along a northwest-southeast axis are compared to time series of B) VIIRS monthly mean sea surface temperature (SST) in degrees Celsius and C) VIIRS monthly mean chlorophyll concentrations (Chl-a) in mg/m3 for areas of upwelling (blue) and wind shadow (red) in False Bay (solid line) and off the Cape Peninsula (dashed line). A dashed grey vertical line indicates where the y-value is 0 and dashed horizontal lines indicate the years. Positive wind speed values indicate south-easterly winds and negative values indicate north-westerly winds (A).

Seasonality was also evident for Chl-a, with a large difference between wind shadow and upwelling areas being found during SE winds, peaking at a difference of 6.9 mg/m$_3$ for the Cape Peninsula regions and 8.1 mg/m$_3$ for the False Bay regions (Fig. 4.8C). A decrease in this difference was seen during winter months when NW winds were more prominent, however, wind shadow regions were

consistently higher in Chl-a with the smallest difference being 0.025 mg/m3 for Cape Peninsula and 0.52 mg/m3 for False Bay and an average difference of 2.1 mg/m3 and 2.8 mg/m3 for the two regions (Fig. 4.8C).

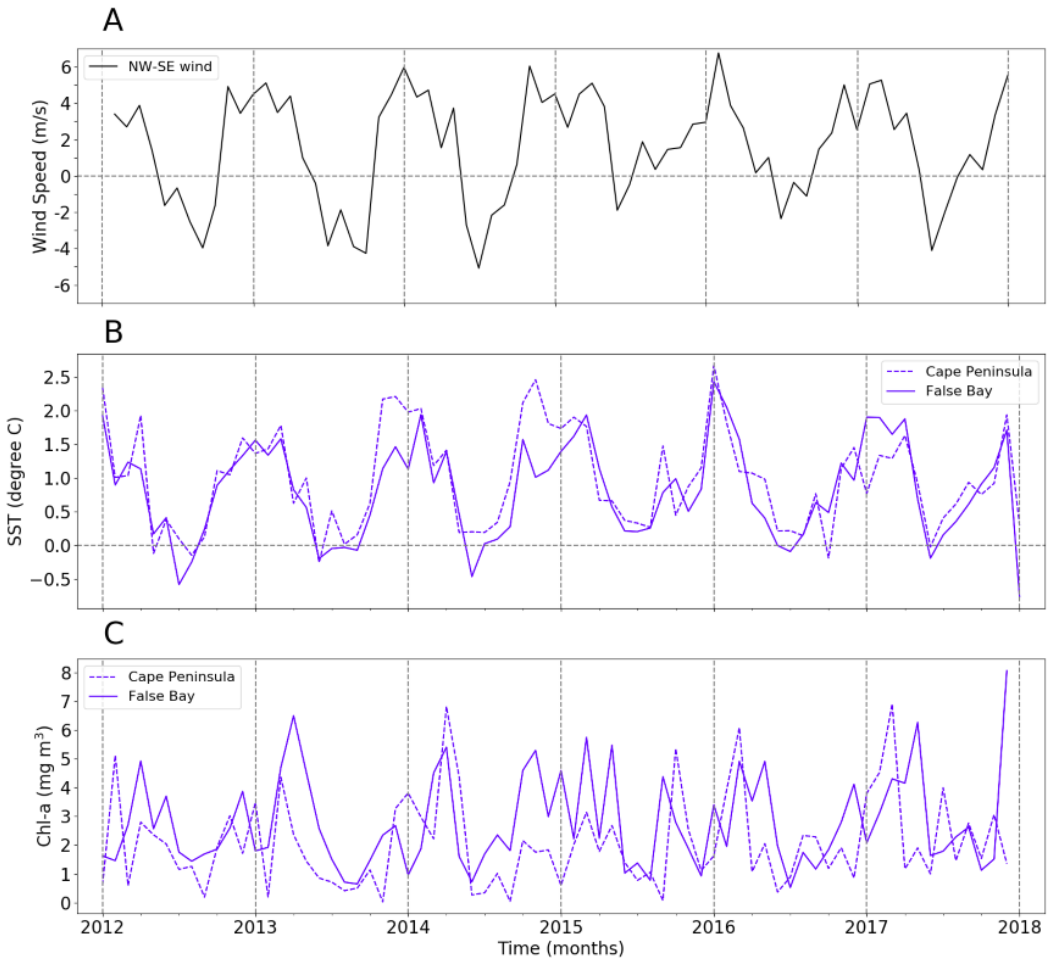


Figure 4.8. A time series of A) ERA-interim v-component wind speeds taken from a location offshore of False Bay (-34.5 S, 18.75 E) rotated along a northwest-southeast axis are compared to the difference between areas of wind shadow and upwelling for B) sea surface temperature (SST) in degrees Celsius and C) chlorophyll concentrations (Chl-a) in mg/m3 for False Bay (solid line) and off the Cape Peninsula (dashed line). A dashed grey vertical line indicates where the y-value is 0 and dashed horizontal lines indicate the years. Positive wind speed values indicate south-easterly winds (upwelling favorable) and negative values indicate north-westerly winds (A).

## 5. DISCUSSION

### 5.1. Wind variability over False Bay and the Cape Peninsula

There was a high spatial variability in the SE winds over False Bay and the Cape Peninsula and this variability was clearly visible in high-resolution SAR images. Within False Bay and off the Cape Peninsula, clear wind shadows were seen during SE winds. Areas of wind acceleration were visible around Cape Hangklip and Cape Point as well as on either side of the wind shadows in both regions. These sharp changes in wind speed were likely the result of vertical compression and a capping of the inversion layer over high mountain ridges as the SAA moves eastward during the SE wind regime. Wind shadows and accelerations in this region have been described previously in other studies (Jury *et* al., 1985a; Jury *et* al., 1985b; Jury, 1987; Jury, 1988), but never with such high spatial resolution as 1 km. These high-resolution SAR images show that even over short distances in coastal regions changes in wind speed can be both rapid and large.

An important outcome of this study is that during SE winds within False Bay and off the Cape Peninsula the typical co-variance often observed between SST and wind speed was absent, whilst the inverse was observed (Nonaka & Xie, 2003; Dorman *et al*., 2006; Chelton *et al*., 2007; Perlin *et al*., 2007; Small *et al*., 2008). Areas of wind shadow corresponded to warmer surface waters whereas strong coastal winds corresponded to areas of low SST and upwelling signals in lee of the mountainous coasts. This pattern was most noticeable in the Cape Peninsula region. This negative relationship between winds and SST shows that in these coastal areas the effects of orography dominates over the thermal feedback effect during the SE wind regime. Through the use of SAR winds, this variability in wind speeds over smaller spatial scales were more easily detectable, allowing us to identify areas where the wind regime is influenced by surrounding topography in coastal regions. Strong wind variability as result of orography could even be seen during light south-easterlies, when average wind speeds over the region were +/- 8 m/s. This high spatial resolution also allows us to get a better understanding of the spatial extent of these orographic effects with notable variability in the orientation and area of the wind shadows in False Bay and off the Cape Peninsula. It is likely that the shape and position of these wind shadows could be influenced by the height of the inversion layer as a deep SE wind develops into a shallow south-easter. Future studies looking at these orographic effects should include vertical wind profiles in order to explore how changes in the depth of the inversion layer as the SE regime develops could affect the intensity and area of wind wakes and wind jets. While it seems that orography primarily affects wind variability at the coast, it should be noted that the thermal feedback effect appears to play a larger role in wind speed further offshore, as stronger winds were observed in areas with higher SST; this is similar to results reported in studies by Nonaka & Xie (2003), Chelton *et al*. (2004), Chelton *et al*. (2007), Small *et al*. (2008).

SAR data have been used to explore coastal winds in other regions around the globe with similar orographic effects being found. Such coastal regions include the North Atlantic coast (Beal & Pichel,

1998), the Norwegian coast (Korsbakken *et al*., 1998; Sanvik & Furevik, 2002), the east coast of the United States (Beal, 2000), Alaska (Monaldo, 2000; Fisher *et al*., 2008), the Bering Sea (Friedman *et* al., 2001) and the west coast of the United States (Li *et al*., 2007). A study by Shimada & Kawamura (2004), with methods similar to the study presented here, used SAR (ERS-1/2) and scatterometer (QuickSCAT) derived wind data in combination to investigate the coastal wind regime off the Pacific coast of northern Japan during the winter monsoon season. Through the use of case studies, they explored the orographic effects on the wind variability during two dominant wind regimes. Wind jets and wind shadows were observed in both the SAR images and QuickSCAT data. These topographically modified winds were a result of gaps and blockages in the coastal mountains and these orographic effects were observed at both large and small spatial scales. The position and extent of these wind jets and wind wakes differed depending on the direction of prevailing winds. Additionally, a connection was found between the minima and maxima of coastal winds and significant wave height, signifying that coastal topography influences not only wind variability but other ocean dynamics such as offshore wind wave development.

The applications of SAR wind data are very promising. A paper on the consensus of SAR wind retrievals from the 2nd Workshop on Coastal and Marine Applications of SAR highlights the progress and potential of SAR wind retrieval in coastal regions in applications relating to weather forecasts, climate modelling and the study of coastal wind dynamics (Monaldo *et al*., 2004). Currently, the accuracy of SAR wind retrieval is up to 2 m/s for winds ranging between 2 to 20 m/s and there is potential for the improvement of these parameters (Monaldo *et al*., 2004).

### 5.2. Measured vs modelled winds

An important outcome of this study was seen in the maps of the difference between SAR derived wind speed and ECMWF modelled wind speed during SE winds. Here it was seen that despite the relatively high spatial resolution of 9 km for this global atmospheric model, ECMWF was still unable to capture the wind variability within this region with large areas of difference between the modelled and measured winds. The majority of these errors occurred in the areas affected by topography, such as areas of wind shadow and wind acceleration. The model seems to overestimate winds in wind shadow zones and under estimate wind speed in the areas where wind acceleration occurred. Although some impact of orography was seen in the ECMWF outputs, with lower wind speeds seen in the northern section of the bay, the way in which the model simulates the impact of orography was incorrect. These findings highlight the importance of adequately accounting for the effect of topography in atmospheric models to study coastal regions.

Other studies have also reported discrepancies in atmospheric and climate model outputs in coastal regions. Such a study, by Cavaleri & Bertotti (2004), looked at ECMWF model outputs for wind speeds and wave heights run at different resolutions in enclosed seas and compared these to *in situ* buoy measurements. Wind speed and wave height were often underestimated. These errors were largely

influenced by fetch differences with error increasing as the distance from the coast decreased. There was also a decrease in error for lower resolution outputs (Cavaleri & Bertotti, 2004). Another study looking at outputs from ECMWF climate reanalysis products over Greenland showed similar errors for climate surface data such as air pressure, precipitation, cloud cover and temperature (Hanna & Valdes, 2001).

### 5.3. Co-variability between wind, SST and Chl-a

Wind variability plays an important role in the ocean dynamics within the Cape Peninsula/ False Bay region. Co-variability was observed during the SE wind regime between the SAR derived wind estimates and the SST data with a decrease in winds corresponding to an increase in temperatures. This relationship was most evident off the Cape Peninsula where areas of warmer SST were seen in the wind shadow zones and a strong upwelling signal was observed in areas of wind acceleration. For False Bay, the relationship between SST and wind seems slightly more complex, with warmer SST observed in the northern half of the bay and cooler SST at the mouth of the bay. This pattern could be explained by wind forcing within the bay. In the wind stress curl images, upwelling was seen on the northern shores of False Bay during strong SE winds with an area of positive Ekman pumping, or downwelling, observed in the wind shadow region. This region of convergence across the bay may act to trap waters in the northern section. Although upwelling is occurring along these shores this upwelled water is initially warm as it finds its origin in the shallow and well mixed waters of the bay (Gründlingh & Largier, 1991). As these waters are advected offshore, they are slowed down by the decrease in wind in the wind wake. As they reach the wind shadow region and downwelling occurs, these coastal waters are likely trapped inshore. These waters would then be recirculated towards the coast allowing coastal waters to warm up. Such a pattern of recirculation would cause significant mixing within the northern section of False Bay. Positive wind stress curl and upwelling that occurred off Cape Hangklip bring cooler waters into the bay. However, the region of convergence in the wind shadow zone would prevent these cooler waters from mixing with the warmer waters in the northern region.

The effects of wind on SST variability off the South African coast is not unknown. A study using numerical modelling showed that variability in SST is closely linked to wind forcing over the southern Benguela upwelling system (Blanke *et al*., 2002). Changes in SST variability were explored by altering the variability of the SAR derived wind speed inputs for a Regional Ocean Modeling System (ROMS). Results showed that ocean surface temperatures were sensitive to changes in wind forcing variability. The authors suggest caution when down scaling the outputs of low-resolution models to smaller scales in coastal regions as the effects of wind forcing offshore may dilute coastal variability (Blanke *et al*., 2002). Wind forcing on ocean surface temperatures is seen all around the globe in coastal regions where upwelling-favorable winds occur (Demarq, 2009.; Hormazaba *et al*., 2001; Rueda-Roa & Muller-Karger, 2013).

In terms of ocean colour, the event-scale co-relationship between wind and Chl-a, or SST and Chl-a, was less evident. It must be noted that the effects of wind on phytoplankton dynamics and response is more complex than the effects between wind and SST. Biological response to physical changes can depend on a combination of factors, some of which could include the nutrient availability, the phytoplankton types and their adaptability to mixing and temperature changes, as well as presence of grazing zooplankton. Still, there was a general coherence in the pattern of chlorophyll observed and the general wind forcing with retention regions associated with higher chlorophyll concentration, and regions of strong winds (associated with mixing and dispersion) showing low Chl-a. Observations over a longer time scale may be needed to better determine how the wind regime may affect Chl-a in this region.

This coherence between warmer waters and higher Chl-a has been observed in previous studies. Barlow (1982) described Chl-a in the southern Benguela during three stages of upwelled water: recently upwelled water (Type 1), maturing upwelled water (Type 2) and aged upwelled water (Type 3). As these upwelled waters matured, inorganic nutrients concentrations decreased and Chl-a increased, with the highest Chl-a being found in the warmer matured upwelled waters (Barlow, 1982). Studies have shown that remote forcing can influence the biology of coastal waters. In Monteray Bay, California, winds play an important role in red tide bloom dynamics (Ryan *et al*., 2009). Similar to False Bay, Monteray Bay is largely influenced by the cycling of upwelling favourable winds, relaxations and reversals. Cold nutrient rich upwelled water is brought into the bay during upwelling favourable winds and warmer offshore waters are advected into the bay during relaxations/ reversals. This results in thermal fronts known as upwelling shadows and creates a bloom incubation area along the north-eastern shores of Monteray Bay (Ryan *et al*., 2009). Another study using satellite data from 1998 to 2007 explored the relationship between SST (AVHRR), chlorophyll concentration (SeaWiFS) and winds (QuickSCAT) in eastern boundary upwelling systems including the Benguela (Demarq, 2009). No significant relationship was found between SST and chlorophyll, however there was a significant relationship between upwelling favorable winds and Chl-a (Demarq, 2009). With the high spatial resolution of SAR winds there is the potential for the increase in the amount of studies on how coastal wind variability can affect primary productivity in upwelling regions.

### 5.4. Seasonality in wind, SST and Chl-a

Clear seasonal patterns were observed in the wind regime, with SE winds dominating in summer and NW winds dominating during winter for each of the 6 years observed. This seasonal cycle coincided with fluctuations in ocean surface temperatures as warmer SST were found during summer months and cooler waters occurred during winter months. Overall, False Bay was warmer than the Cape Peninsula side. This could be a result of water retention within False Bay as explained in section 5.2. Upwelling and wind shadows occurred in a less confined space and over a steeper bathymetry on the Cape Peninsula side resulting in a stronger upwelling signal. Additionally, upwelling zones in both regions were cooler than wind shadow areas with this difference in temperature decreasing during

winter months as a predominantly NW wind regime occurs and fewer SE winds blow. Within this region, SE winds favour upwelling which may explain the matching fluctuations in winds and SST.

Seasonal patterns were also observed in Chl-a with peaks during SE summer regime and troughs during NW winter regimes. Similar seasonal patterns in SST and Chl-a have been described in this region. Weeks *et al*. (2006) used a time series spanning six years (1998-2003) of high-resolution satellite data (1 km) for SST (AVHRR) and chlorophyll (SeaWiFS) to explore variability in temperature and primary production in the southern Benguela upwelling region. Bathymetry played an important role in driving some of the spatial variability in the upwelling with cooler waters found at steeper bathymetries. Weeks *et al,* (2006) found that within the Cape Peninsula region, there was a strong seasonal signal in temperature and upwelling indices. A decrease in SST and increase in upwelling occurred during spring or summer months (Weeks *et al*., 2006), similar to what was seen in the study presented here where a larger difference was found between upwelling and wind shadow regions during summer in the 2012-2017 time series for VIIRS data.

The main observation for ocean colour was that Chl-a were not highest directly in the upwelling zones but rather in the retention zones. This is in agreement with the Weeks *et al*., (2006) findings where off the Cape Peninsula, fluctuations in Chl-a along the inner shelf matched those of SST whereas further offshore Chl-a were consistently higher than inshore (Weeks *et al*., 2006). The results from these studies highlights the importance of the use of high spatial resolution data when exploring variability in surface temperatures and Chl-a in coastal regions.

### 5.5. Limitations and suggestions for further research

Although SAR data have a high spatial resolution, its temporal resolution is still rather low in comparison to other wind speed products. Due to this, the amount of days where SAR data were available was limited. This resulted in the use of case studies to explore the wind regime rather than a synoptic view of wind variability during the SE regime.

Further studies are required to explore wind variability and wind forcing over the coastal region of False Bay and the Cape Peninsula, and a larger data set over an increased time period is needed to better quantitatively define wind variability over the area. Future studies could look at the potential of exploiting SAR surface signatures to gain insight on the vertical wind profile by combining SAR observations with vertical soundings made at Cape Town International Airport. Additionally, the ability of SAR satellites to collect data near the coast also opens up the possibility to explore other ocean dynamics affected by wind, specifically circulation, and future studies should include the effects of currents within this region when exploring both SST and Chl-a variability.

## 6. CONCLUSION

Coastal zones are some of the most productive regions in the world and are where most of human interaction with the sea takes place. Despite this importance, many of the ocean-atmosphere dynamics within these areas are understudied, likely due to the lack of high-resolution data and data loss due to land contamination (Johannessen, 2000). Due to this, coastal wind phenomena that are often described have not yet been studied. The results from this study shows that high-resolution SAR wind estimates can be used to explore wind variability in the coastal regions of False Bay and the Cape Peninsula. Here, the effects of orography play a large role in the variability of the predominantly SE wind regime with high mountains ridges creating both wind acceleration and wind wakes in their lee. These varying winds can also influence SST and Chl-a in these bays. Warmer waters were found in wind shadow regions and colder upwelled waters were observed in areas of strong winds. There was some correspondence between decreased winds and higher Chl-a, and increased winds and lower Chl-a. However, this relationship was not as distinct as with wind and SST. Biology is more complex and is influenced by a large number of factors and more studies are required to explore the long-term effects of wind variability on Chl-a. Finally, the outcomes of this study showed that global atmospheric models, such as ECMWF, do not accurately predict winds in this region. These models need to better incorporate the effects of surrounding topography on the wind regime in order to accurately predict these coastal winds, and in turn wind forcing. The use of high-resolution SAR winds as an input for such atmospheric models could help to resolve these problems and allow for the output of more accurate coastal wind predictions. The increase in SAR acquisitions globally and the transition to an open data policy as a result of the Sentinel-1 missions will open greater possibilities for the application of SAR imagery in coastal ocean physics.

**REFERENCES**

Atkins, G. R. 1970a. Thermal structure and salinity of False Bay. *Transactions of the Royal Society of South Africa*, *39*(2), 117-128.

Atkins, G. R. 1970b. Winds and current patterns in False Bay. *Transactions of the Royal Society of South Africa*, *39*(2), 139-148.

Ballegooyen, R. 1991. The dynamics relevant to the modelling of synoptic scale circulations within False Bay. *Transactions of the Royal Society of South Africa*, *47*(4), 419-432.

Barlow, R. G. 1982. Phytoplankton ecology in the southern Benguela current. I. Biochemical composition. *Journal of Experimental Marine Biology and Ecology*, *63*(3), 209-227.

Beal, R. C. 2000. Toward an international stormwatch using wide swath SAR. *Johns Hopkins APL technical digest*, *21*(1), 12-20.

Beal, R. C., & Pichel, W. G. 1998. StormWatch 97-98 and beyond: application of SAR as a high resolution scatterometer in coastal regions, in *IGARSS '98. Sensing and managing the Environment. 1998 IEEE International Geoscience and Remote Sensing. Symposium Proceedings. (Cat. No.98CH36174).* Seattle: John Hopkins University, 3, 1379-1381.

Blanke, B., Roy, C., Penven, P., Speich, S., McWilliams, J., & Nelson, G. 2002. Linking wind and interannual upwelling variability in a regional model of the southern Benguela. *Geophysical Research Letters*, *29*(24).

Castelao, R. M., Barth, J. A., & Mavor, T. P. 2005. Flow-topography interactions in the northern California Current System observed from geostationary satellite data. *Geophysical research letters*, *32*(24).

Cavaleri, L., & Bertotti, L. 2004. Accuracy of the modelled wind and wave fields in enclosed seas. *Tellus A: Dynamic Meteorology and Oceanography*, *56*(2), 167-175.

Chelton, D. B., Schlax, M. G., Freilich, M. H., & Milliff, R. F. 2004. Satellite measurements reveal persistent small-scale features in ocean winds. S*cience*, *303*(5660), 978-983.

Chelton, D. B., Schlax, M. G., & Samelson, R. M. 2007. Summertime coupling between sea surface temperature and wind stress in the California Current System. *Journal of Physical Oceanography*, *37*(3), 495-517.

Cram, D. L. 1970. A suggested origin for the cold surface water in central False Bay. *Transactions of the Royal Society of South Africa*, *39*(2), 129-137.

Dagestad, K. F., Horstmann, J., Mouche, A., Perrie, W., Shen, H., Zhang, B., ... & Badger, M. 2013. Wind retrieval from synthetic aperture radar-an overview, in *4th SAR Oceanography Workshop (SEASAR 2012): Advances in SAR Oceanography*. European Space Agency.

Danilo, C., Chapron, B., Mouche, A., Garello, R., & Collard, F. 2007. Comparisons between HF radar and SAR current measurements in the Iroise Sea. In *OCEANS 2007-Europe.* Aberdeen, 1-5.

Dee, D. P., Uppala, S. M., Simmons, A. J., Berrisford, P., Poli, P., Kobayashi, S., ... & Bechtold, P. 2011. The ERA-Interim reanalysis: Configuration and performance of the data assimilation system. *Quarterly Journal of the royal meteorological society*, *137*(656), 553-597.

Demarcq, H. 2009. Trends in primary production, sea surface temperature and wind in upwelling systems (1998–2007). *Progress in Oceanography*, *83*(1-4), 376-385.

Demarcq, H., Barlow, R. G., & Shillington, F. A. 2003. Climatology and variability of sea surface temperature and surface chlorophyll in the Benguela and Agulhas ecosystems as observed by satellite imagery. *African Journal of Marine Science*, *25*(1), 363-372.

Diab, R. D., & Garstang, M. 1984. Assessment of wind power potential for two contrasting coastlines of South Africa using a numerical model. *Journal of climate and applied meteorology*, *23*(12), 1645-1659.

DiMarco, S. F., Chapman, P., & Nowlin Jr, W. D. 2000. Satellite observations of upwelling on the continental shelf south of Madagascar. *Geophysical Research Letters*, *27*(24), 3965-3968.

Dorman, C. E., Dever, E. P., Largier, J., & Koračin, D. 2006. Buoy measured wind, wind stress and wind stress curl over the shelf off Bodega Bay, California. *Deep Sea Research Part II: Topical Studies in Oceanography*, *53*(25-26), 2850-2864.

Doyle, J. D. 1997. The influence of mesoscale orography on a coastal jet and rainband. *Monthly Weather Review*, *125*(7), 1465-1488.

Dufois, F., & Rouault, M. 2012. Sea surface temperature in False Bay (South Africa): towards a better understanding of its seasonal and inter-annual variability. *Continental Shelf Research*, *43*, 24-35.

Fisher, C. M., Young, G. S., Winstead, N. S., & Haqq-Misra, J. D. 2008. Comparison of synthetic aperture radar–derived wind speeds with buoy wind speeds along the mountainous Alaskan coast. *Journal of Applied Meteorology and Climatology*, *47*(5), 1365-1376.

Friedman, K. S., Sikora, T. D., Pichel, W. G., Clemente-Colón, P., & Hufford, G. 2001. Using spaceborne synthetic aperture radar to improve marine surface analyses. *Weather and forecasting*, *16*(2), 270-276.

Gagliardini, D. A., Clemente-Colón, P., Bava, J., Milovich, J. A., & Frulla, L. A. 2001. Complementary use of SAR and thermal IR observations in the Brazil-Malvinas confluence region. *Canadian journal of remote sensing*, *27*(6), 643-650.

Gründlingh, M. L., Hunter, I. T., & Potgieter, E. 1989. Bottom currents at the entrance to False Bay, South Africa. *Continental shelf research. Oxford, New York NY*, *9*(12), 1029-1048.

Gründlingh, M. L., & Largier, J. L. 1991. Physical oceanography of False Bay: a review. *Royal Society of South Africa. Transactions TRSAAC*, *47*(4|5).

Hanna, E., & Valdes, P. 2001. Validation of ECMWF (re) analysis surface climate data, 1979–1998, for Greenland and implications for mass balance modelling of the ice sheet. *International Journal of Climatology: A Journal of the Royal Meteorological Society*, *21*(2), 171-195.

Hasager, C. B., Nielsen, M., Astrup, P., Barthelmie, R., Dellwik, E., Jensen, N. O., ... & Furevik, B. R. 2005. Offshore wind resource estimation from satellite SAR wind field maps. *Wind Energy: An International Journal for Progress and Applications in Wind Power Conversion Technology*, *8*(4), 403-419.

Holt, B. 2004. SAR imaging of the ocean surface. *Synthetic aperture radar marine user's manual*, 25-80.

Hormazabal, S., Shaffer, G., Letelier, J., & Ulloa, O. 2001. Local and remote forcing of sea surface temperature in the coastal upwelling system off Chile. *Journal of Geophysical Research: Oceans*, *106*(C8), 16657-16671.

Horstman, D. A., McGibbon, S., Pitcher, G. C., Calder, D., Hutchings, L., & Williams, P. 1991. Red tides in False Bay, 1959-1989, with particular reference to recent blooms of Gymnodinium sp. *Transactions of the Royal Society of South Africa*, *47*(4), 611-628.

Hsu, M. K., Liu, A. K., & Liu, C. 2000. A study of internal waves in the China Seas and Yellow Sea using SAR. *Continental shelf research*, *20*(4-5), 389-410.

Jackson, P. L., Mayr, G., & Vosper, S. 2013. Dynamically-driven winds, in Chow F., De Wekker S., Snyder B. (eds). *Mountain weather research and forecasting.* Springer, Dordrecht. 121-218

Jacobson, M. 2014. The influence of a spatially varying wind field on the circulation and thermal structure of False Bay during summer: a numerical modelling study. BSc (Hons) Thesis, Cape Town, University of Cape Town.

Jin, X., Dong, C., Kurian, J., McWilliams, J. C., Chelton, D. B., & Li, Z. 2009. SST–wind interaction in coastal upwelling: Oceanic simulation with empirical coupling. *Journal of Physical Oceanography*, *39*(11), 2957-2970.

Johannessen, J. A. 2000. Coastal observing systems: The role of synthetic aperture radar. *Johns Hopkins APL Technical Digest*, *21*(1), 41-48.

Jury, M.R., 1980. Characteristics of summer wind fields and air sea interactions over the Cape Peninsula upwelling region. MSc Thesis, Cape Town, University of Cape Town.

Jury, M. R. 1985. Mesoscale variations in summer winds over the Cape Columbine—St Helena Bay region, South Africa. *South African Journal of Marine Science*, *3*(1), 77-88.

Jury, M. R. 1987. Aircraft observations of meteorological conditions along Africa's West Coast between 30–35 South. *Journal of climate and applied meteorology*, *26*(11), 1540-1552.

Jury, M. R. 1988. A climatological mechanism for wind-driven upwelling near Walker Bay and Danger Point, South Africa. *South African Journal of Marine Science*, *6*(1), 175-181.

Jury, M. 1991. The weather of False Bay. *Royal Society of South Africa. Transactions TRSAAC, 47*(4|5).

Jury, M. R., Kamstra, F., & Taunton-Clark, J. 1985a. Diurnal wind cycles and upwelling off the northern portion of the Cape Peninsula in summer. *South African Journal of Marine Science*, *3*(1), 1-10.

Jury, M. R., Kamstra, F., & Taunton-Clark, J. 1985b. Synoptic summer wind cycles and upwelling off the southern portion of the Cape Peninsula. *South African Journal of Marine Science*, *3*(1), 33-42.

Korsbakken, E., Johannessen, J. A., & Johannessen, O. M. 1998. Coastal wind field retrievals from ERS synthetic aperture radar images. *Journal of Geophysical Research: Oceans*, *103*(C4), 7857-7874.

Krug, M., Schilperoort, D., Collard, F., Hansen, M. W., & Rouault, M. 2018. Signature of the Agulhas Current in high resolution satellite derived wind fields. *Remote Sensing of Environment*, *217*, 340-351.

Kuo, N. J., Zheng, Q., & Ho, C. R. 2000. Satellite observation of upwelling along the western coast of the South China Sea. *Remote sensing of environment*, *74*(3), 463-470.

Lehner, S., Schulz-Stellenfleth, J., Schattler, B., Breit, H., & Horstmann, J. 2000. Wind and wave measurements using complex ERS-2 SAR wave mode data. *IEEE Transactions on Geoscience and Remote Sensing*, *38*(5), 2246-2257.

Li, X., Zheng, W., Pichel, W. G., Zou, C. Z., & Clemente-Colón, P. 2007. Coastal katabatic winds imaged by SAR. *Geophysical research letters*, *34*(3).

Li, X., Zhao, Z., & Pichel, W. G. 2008. Internal solitary waves in the northwestern South China Sea inferred from satellite images. *Geophysical Research Letters*, *35*(13).

Liu, A. K., & Hsu, M. K. 2004. Internal wave study in the South China Sea using synthetic aperture radar (SAR). *International Journal of Remote Sensing*, *25*(7-8), 1261-1264.

Long, D. G., & Skouson, G. B. 1996. Calibration of spaceborne scatterometers using tropical rain forests. *IEEE Transactions on Geoscience and Remote Sensing*, *34*(2), 413-424.

Lutjeharms, J. R. E., Olivier, J., & Lourens, E. 1991. Surface fronts of False Bay and vicinity. *Royal Society of South Africa. Transactions TRSAAC*, *47*(4|5).

McCandless, S. W., & Jackson, C. R. 2004. Principles of synthetic aperture radar. *SAR Marine User's Manual*, 1-23.

Monaldo, F. 2000. The Alaska SAR demonstration and near-real-time synthetic aperture radar winds. *Johns Hopkins APL Technical Digest*, *21*(1), 75-79.

Monaldo, F. M., Thompson, D. R., Beal, R. C., Pichel, W. G., & Clemente-Colón, P. 2001. Comparison of SAR-derived wind speed with model predictions and ocean buoy measurements. *IEEE Transactions on Geoscience and Remote Sensing*, *39*(12), 2587-2600.

Monaldo, F. M., & Beal, R. 2004. Wind speed and direction. *SAR Marine User's Manual*, 305-320.

Monaldo, F., Kerbaol, V., Clemente-Colon, P., Furevik, B., Hortsmann, J., Johannessen, J., Li, X., Pichel, W., Sikora, T., Thompson, D., & Wackerman, C. 2004. The SAR measurement of ocean surface winds: an overview for the 2nd workshop on coastal and marine applications of SAR, in *Proceedings of the Second Workshop on SAR Coastal and Marine Applications of SAR.* Spitsbergen, 15-32.

Nonaka, M., & Xie, S. P. 2003. Covariations of sea surface temperature and wind over the Kuroshio and its extension: Evidence for ocean-to-atmosphere feedback. *Journal of climate*, *16*(9), 1404-1413.

O'Neill, L. W., Chelton, D. B., & Esbensen, S. K. 2003. Observations of SST-induced perturbations of the wind stress field over the Southern Ocean on seasonal timescales. *Journal of Climate*, *16*(14), 2340-2354.

Perlin, N., Skyllingstad, E. D., Samelson, R. M., & Barbour, P. L. 2007. Numerical simulation of air–sea coupling during coastal upwelling. *Journal of Physical Oceanography*, *37*(8), 2081-2093.

Pitcher, G. C., & Calder, D. 2000. Harmful algal blooms of the southern Benguela Current: a review and appraisal of monitoring from 1989 to 1997. *African Journal of Marine Science*, *22*.

Pitcher, G. C., Bernard, S., & NTULI, J. 2008. Contrasting bays and red tides in the southern Benguela upwelling system. *Oceanography*, *21*(3), 82-91.

Pitcher, G. C., Figueiras, F. G., Hickey, B. M., & Moita, M. T. 2010. The physical oceanography of upwelling systems and the development of harmful algal blooms. *Progress in Oceanography*, *85*(1-2), 5-32.

Qazi, W. A., Emery, W. J., & Fox-Kemper, B. 2014. Computing ocean surface currents over the coastal California current system using 30-min-lag sequential SAR images. *IEEE Transactions on Geoscience and Remote Sensing*, *52*(12), 7559-7580.

Ramanantsoa, J. D., Krug, M., Penven, P., Rouault, M., & Gula, J. 2018. Coastal upwelling south of Madagascar: Temporal and spatial variability. *Journal of Marine Systems*, *178*, 29-37.

Renault, L., Hall, A., & McWilliams, J. C. 2016. Orographic shaping of US West Coast wind profiles during the upwelling season. *Climate dynamics*, *46*(1-2), 273-289.

Risien, C. M., Reason, C. J. C., Shillington, F. A., & Chelton, D. B. 2004. Variability in satellite winds over the Benguela upwelling system during 1999–2000. *Journal of Geophysical Research: Oceans*, *109*(C3).

Rouault, M. J., Mouche, A., Collard, F., Johannessen, J. A., & Chapron, B. 2010. Mapping the Agulhas Current from space: An assessment of ASAR surface current velocities. *Journal of Geophysical Research: Oceans*, *115*(C10).

Rueda-Roa, D. T., & Muller-Karger, F. E. 2013. The southern Caribbean upwelling system: Sea surface temperature, wind forcing and chlorophyll concentration patterns. *Deep Sea Research Part I: Oceanographic Research Papers*, *78*, 102-114.

Ryan, J. P., Fischer, A. M., Kudela, R. M., Gower, J. F., King, S. A., Marin III, R., & Chavez, F. P. 2009. Influences of upwelling and downwelling winds on red tide bloom dynamics in Monterey Bay, California. *Continental Shelf Research*, *29*(5-6), 785-795.

Sandvik, A. D., & Furevik, B. R. 2002. Case study of a coastal jet at Spitsbergen—Comparison of SAR-and model-estimated wind. *Monthly Weather Review*, *130*(4), 1040-1051.

Sentinel-1 SAR User Guide, ESA. https://sentinel.esa.int/web/sentinel/user-guides/sentinel-1-sar/acquisition-modes/interferometric-wide-swath.

Shannon, L. V., Walters, N. M., & Moldan, A. G. S. 1982. The measurement of organic pollution of the sea using satellite imagery. *Water Science and Technology*, *14*(9-11), 1586-1587.

Shannon, L. V., Walters, N. M., & Moldan, A. G. S. 1983. Some features in two Cape bays as deduced from satellite ocean-colour imagery. *South African Journal of Marine Science*, *1*(1), 111-122.

Shannon, L. V., Hennig, H. F. K. O., Shillington, F. A., Bartels, A., & Swart, D. H. 1991. Colour fronts in False Bay: origin, development and implications. *Royal Society of South Africa. Transactions TRSAAC*, *47*(4/5).

Shimada, T., & Kawamura, H. 2004. Wind jets and wind waves off the Pacific coast of northern Japan under winter monsoon captured by combined use of scatterometer, synthetic aperture radar, and altimeter. *Journal of Geophysical Research: Oceans*, *109*(C12).

Small, R. J., Xie, S. P., O'Neill, L., Seo, H., Song, Q., Cornillon, P., ... & Minobe, S. 2008. Air–sea interaction over ocean fronts and eddies. *Dynamics of Atmospheres and Oceans*, *45*(3-4), 274-319.

Smith, R. B. 1982. Synoptic observations and theory of orographically disturbed wind and pressure. *Journal of the Atmospheric Sciences*, *39*(1), 60-70.

Spargo, P. 1991. False Bay, South-Africa – an historic and scientific overview. *Transactions of the Royal Society of South Africa*, *47*, 363-375.

Takeyama, Y., Ohsawa, T., Kozai, K., Hasager, C. B., & Badger, M. 2013). Comparison of geophysical model functions for SAR wind speed retrieval in Japanese coastal waters. *Remote Sensing*, *5*(4), 1956-1973.

Taljaard, S. 1991. The origin and distribution of dissolved nutrients in False Bay. *Royal Society of South Africa. Transactions TRSAAC,*, *47*(4/5).

Tokinaga, H., Tanimoto, Y., & Xie, S. P. 2005. SST-induced surface wind variations over the Brazil–Malvinas confluence: Satellite and in situ observations. *Journal of climate*, *18*(17), 3470-3482.

Tomczak, M., & Godfrey, J. S. 2013. *Regional oceanography: an introduction*. Elsevier.

Vachon, P. W., Chunchuzov, I., & Dobson, F. W. 1998. Wind field structure and speed from RADARSAT SAR images. *Earth Observation Quarterly*, *59*, 12-15.

Van Foreest, D., & Jury, M. R. 1985. A numerical-model of the wind-driven circulation in False Bay. *South African Journal of Science*, *81*(6), 312-317.

Wainman, C. K., Polito, A., & Nelson, G. 1987. Winos and subsurface currents in the False Bay region, South Africa. *South African Journal of Marine Science*, *5*(1), 337-346.

Waldron, H. N., Wainman, C. K., Waldron, M. E., Whittle, C., & Brundrit, G. B. 2008. A prominent colour front in False Bay, South Africa: Cross-frontal structure, composition and origin. *Estuarine, Coastal and Shelf Science*, *77*(4), 614-622.

Wang, Y., Castelao, R. M., & Yuan, Y. 2015. Seasonal variability of alongshore winds and sea surface temperature fronts in Eastern Boundary Current Systems. *Journal of Geophysical Research: Oceans*, *120*(3), 2385-2400.

Weeks, S. J., Barlow, R., Roy, C., & Shillington, F. A. 2006. Remotely sensed variability of temperature and chlorophyll in the southern Benguela: upwelling frequency and phytoplankton response. *African Journal of Marine Science*, *28*(3-4), 493-509.

Yelland, M., & Taylor, P. K. 1996. Wind stress measurements from the open ocean. *Journal of Physical Oceanography*, *26*(4), 541-558.

**APPENDICES**

# APPENDIX A
## SAR Wind Speeds

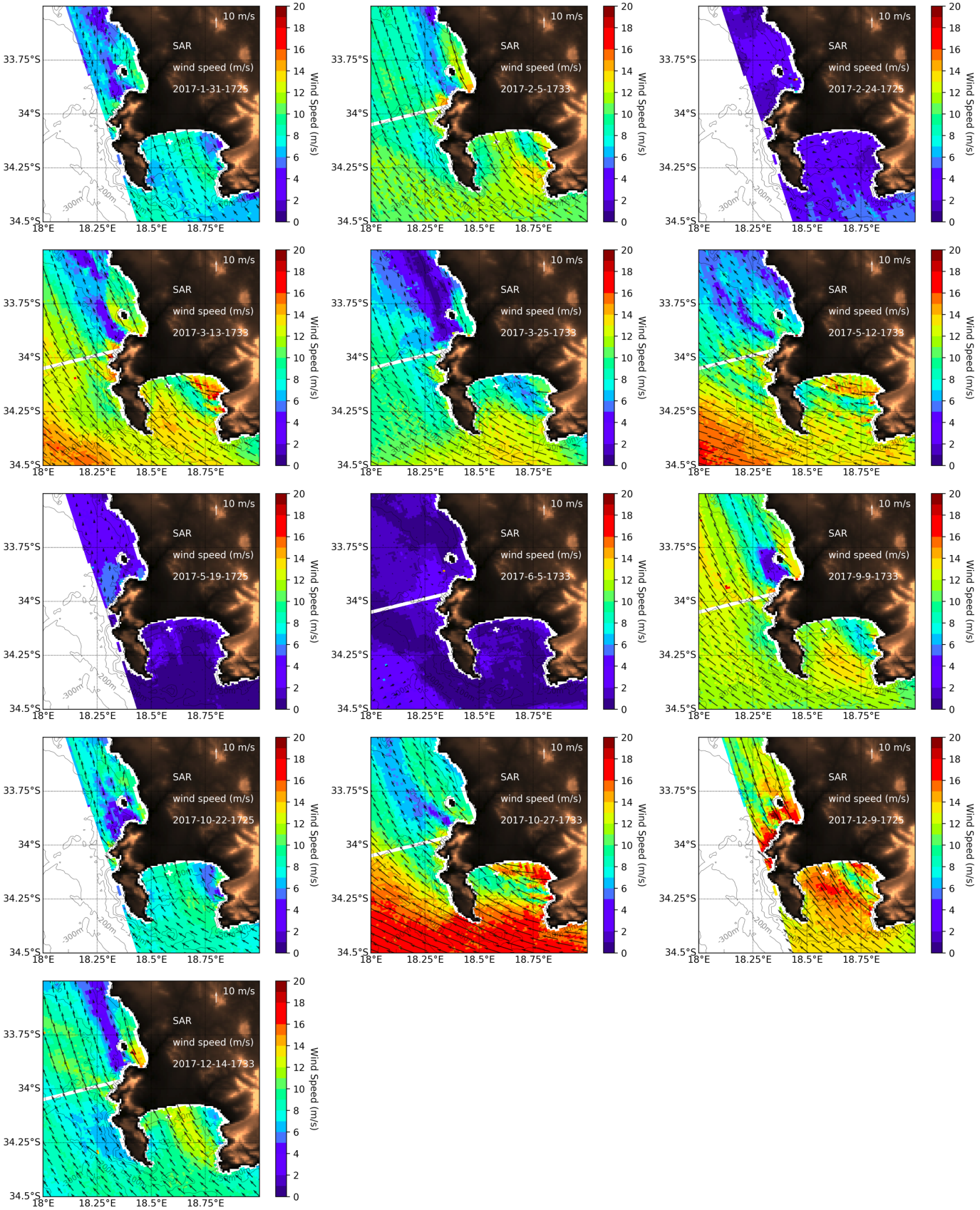


SAR derived wind speeds in m/s several cases of south-easterly (SE) winds over False Bay and the Cape Peninsula. The length of the arrows depicts SAR derived wind speeds and the orientation of the arrow show ECMWF modelled wind direction.

# APPENDIX B

## ECMWF Modelled Wind Speeds

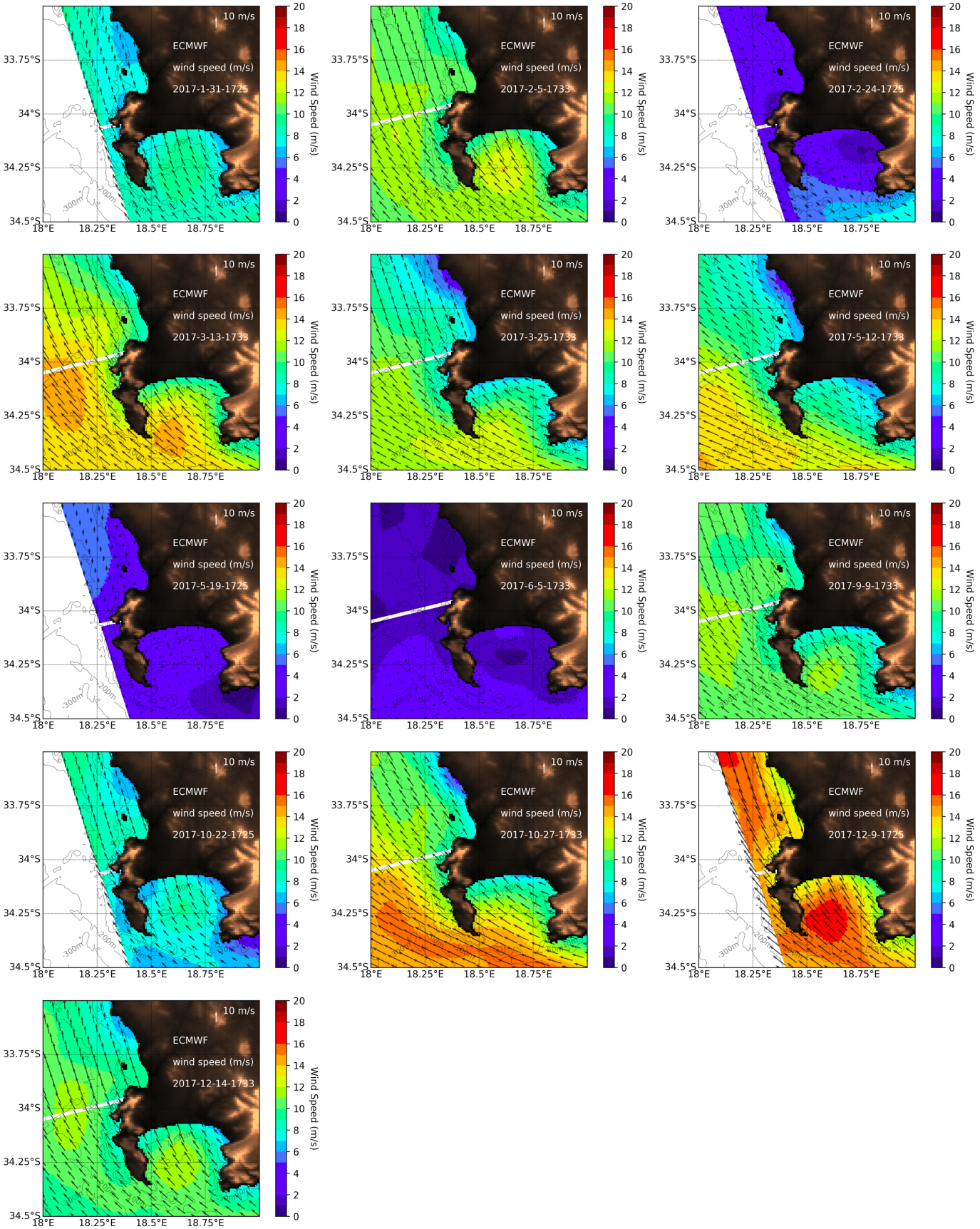


ECMWF modelled wind speeds in m/s for several cases of south-easterly (SE) winds over False Bay and the Cape Peninsula. The length of the arrows depicts wind speeds and the orientation of the arrow show wind direction.

# APPENDIX C
## Difference Between SAR and ECMWF Wind Speeds

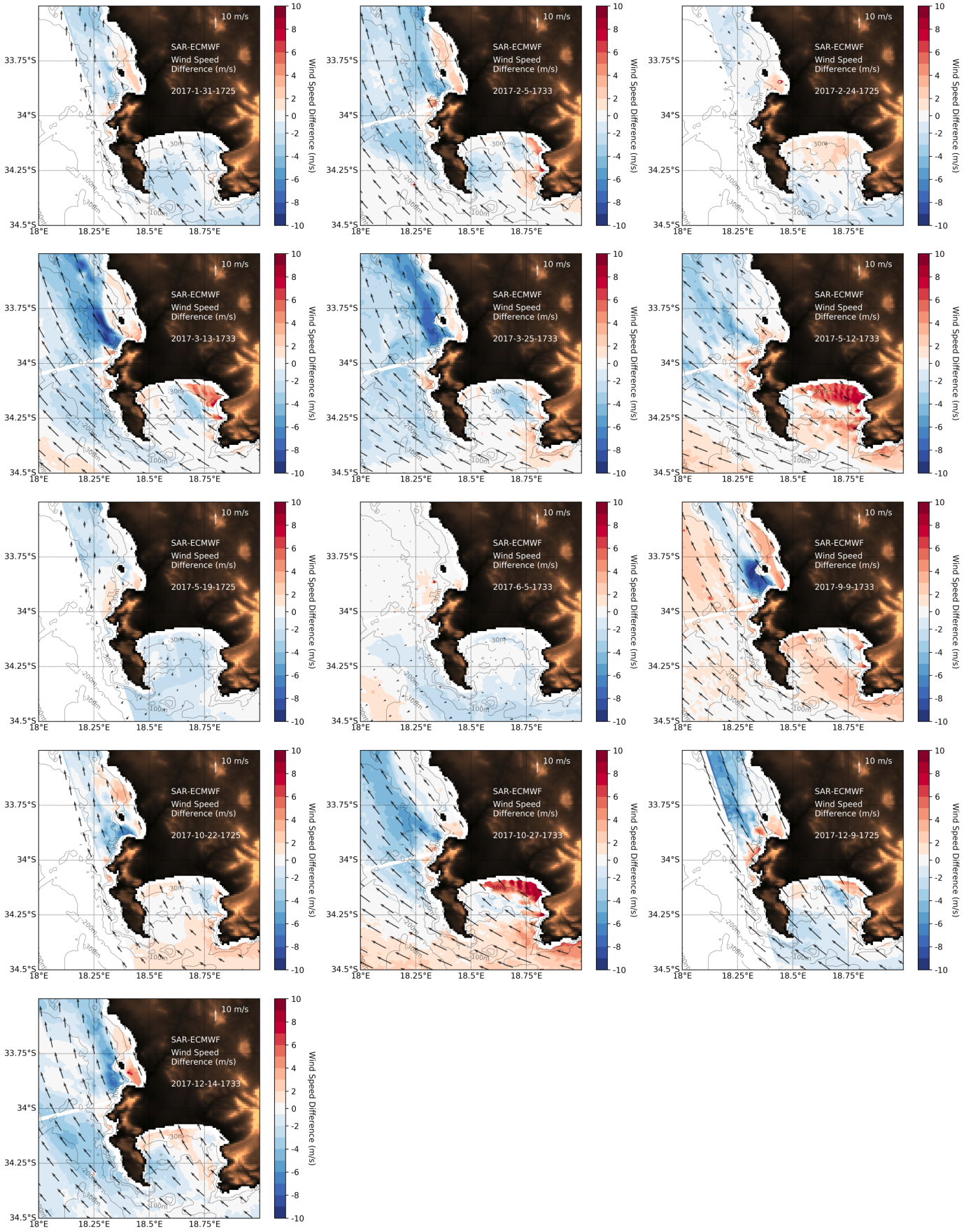


The difference between SAR derived wind speeds and ECMWF modelled wind speeds for several cases of south-easterly (SE) winds over False Bay and the Cape Peninsula with SAR wind vectors overlaid as arrows. The length of the arrows depicts SAR derived wind speeds and the orientation of the arrow show ECMWF modelled wind direction.

# APPENDIX D

## Ekman PumpingDerived from SAR

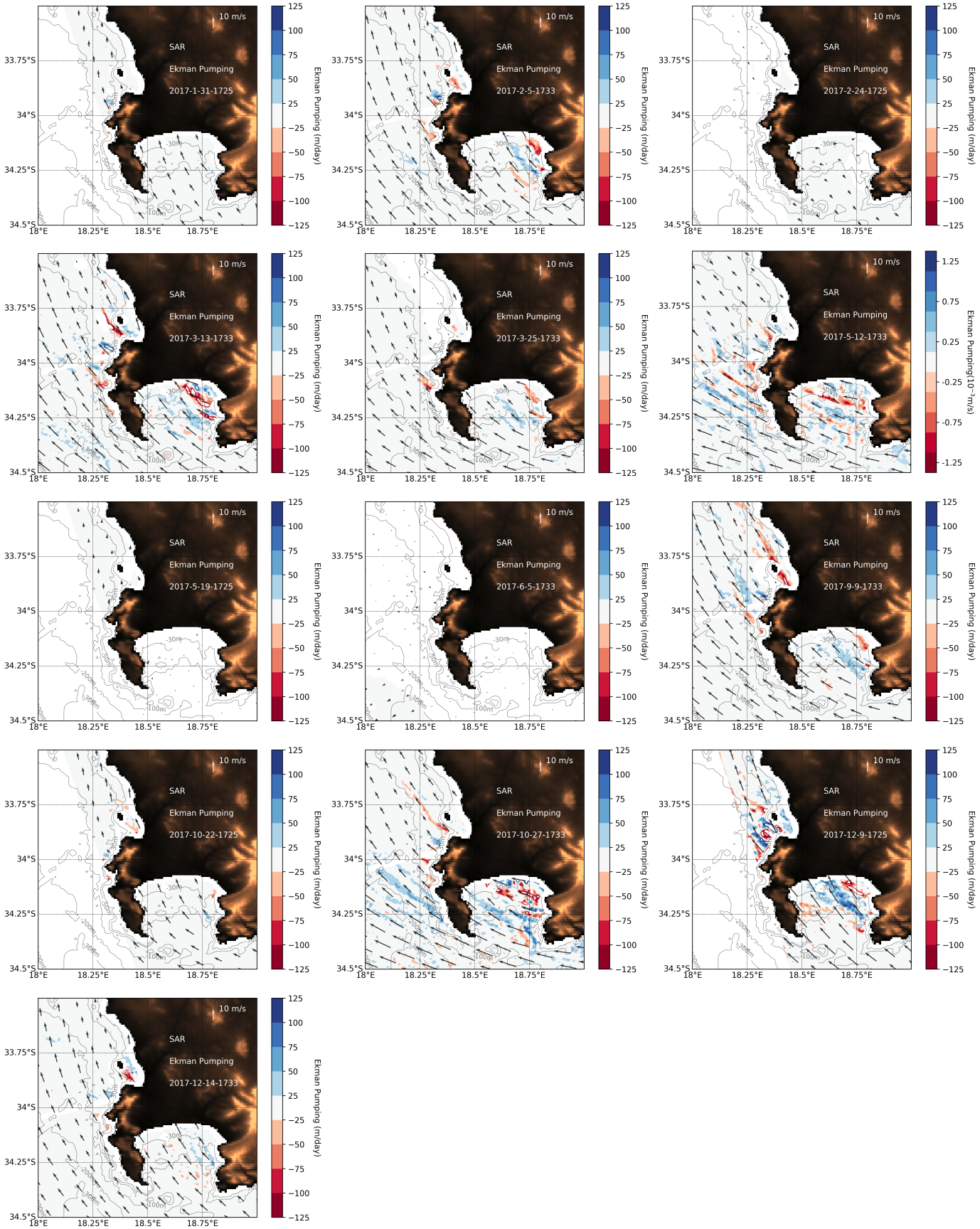


Ekman pumping maps in m/day over False Bay and the Cape Peninsula during several cases of south-easterly (SE) wind with SAR wind vectors overlaid as arrows. Arrow length indicates SAR derived wind speed in m/s and arrow direction indicates ECMWF modelled wind direction.

# APPENDIX F
## VIIRS Sea Surface Temperature Maps

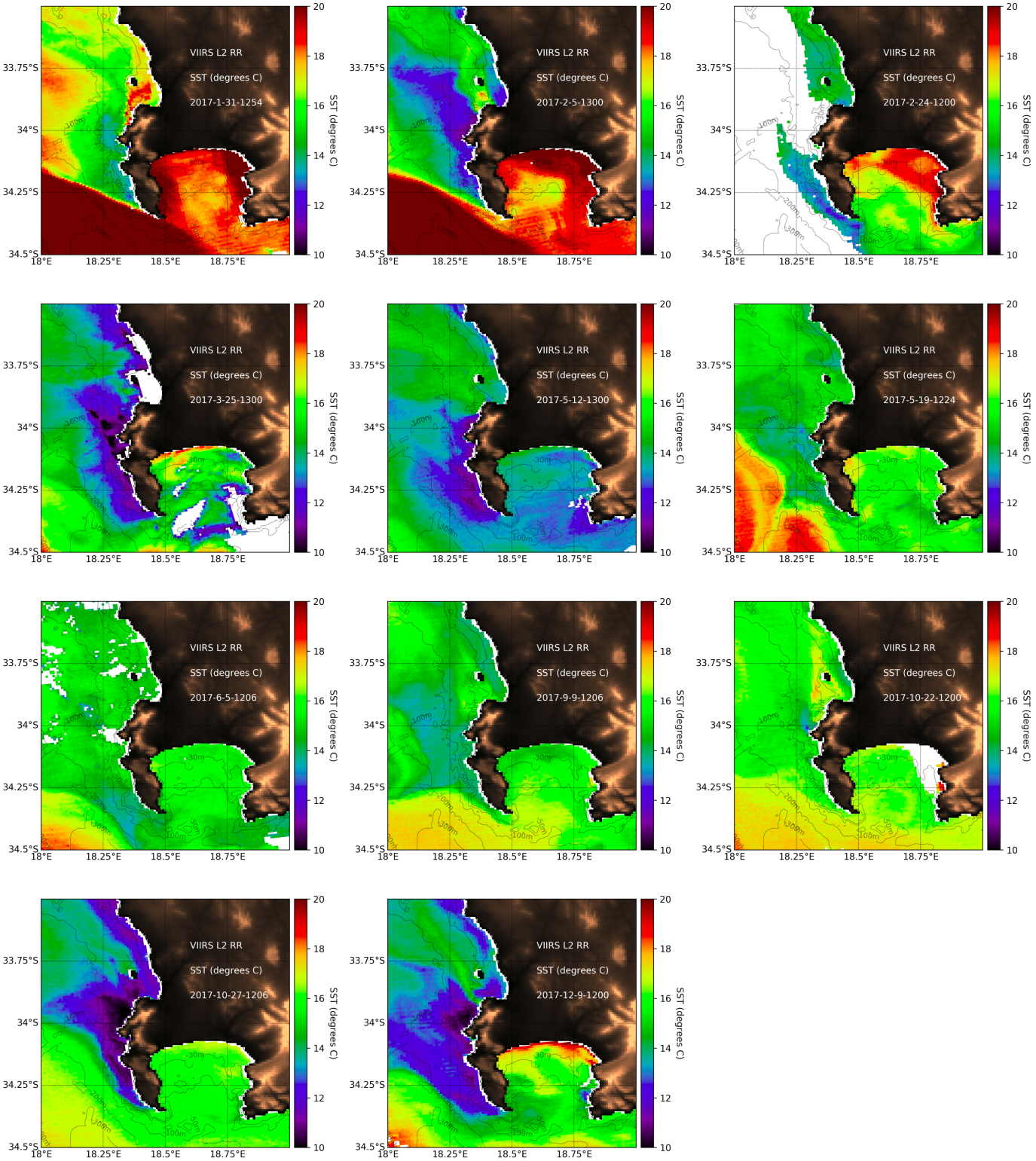


VIIRS sea surface temperature (SST) maps in degrees Celsius (degrees C) for several cases of south-easterly (SE) winds in False Bay and the Cape Peninsula.

# APPENDIX F
## VIIRS Chlorophyll Concentration Maps

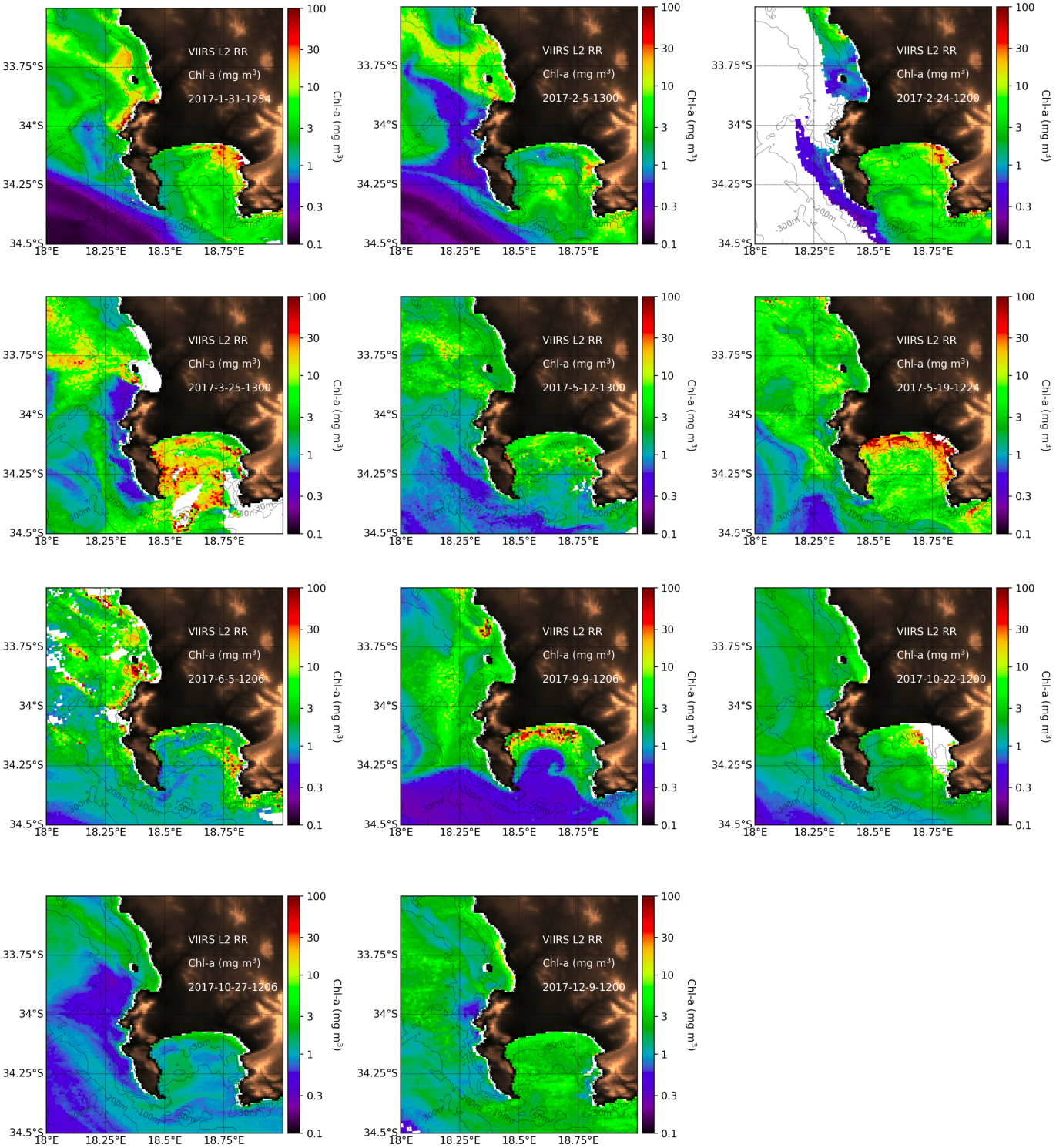


VIIRS chlorophyll concentration (Chl-a) maps in mg/m3 for several cases of south-easterly (SE) winds in False Bay and the Cape Peninsula.

# APPENDIX G
## MODIS Sea Surface Temperature Maps

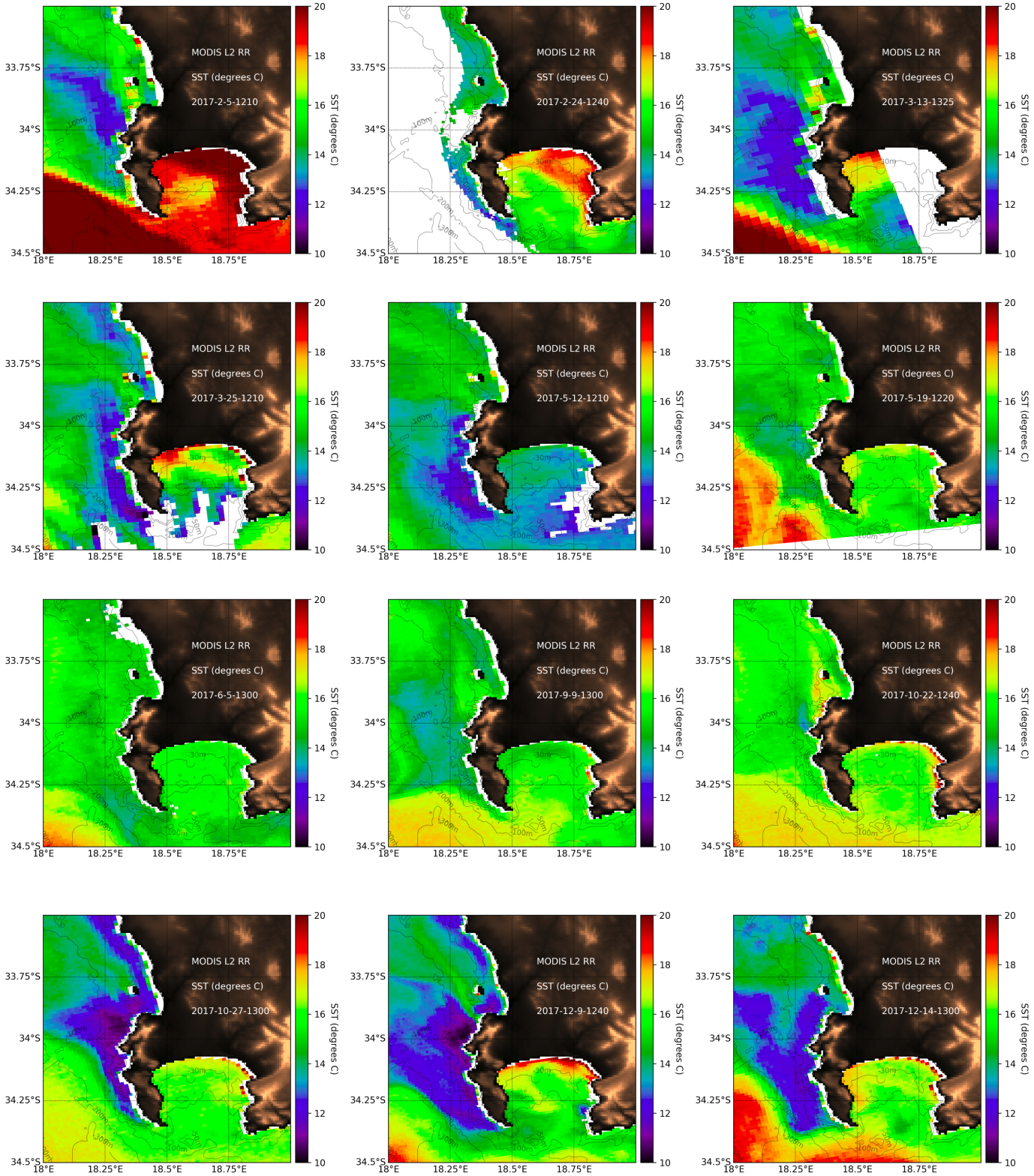


MODIS sea surface temperature (SST) maps in degrees Celsius (degrees C) for several cases of south-easterly (SE) winds in False Bay and the Cape Peninsula.

# APPENDIX H
## MODIS Chlorophyll Concentration Maps

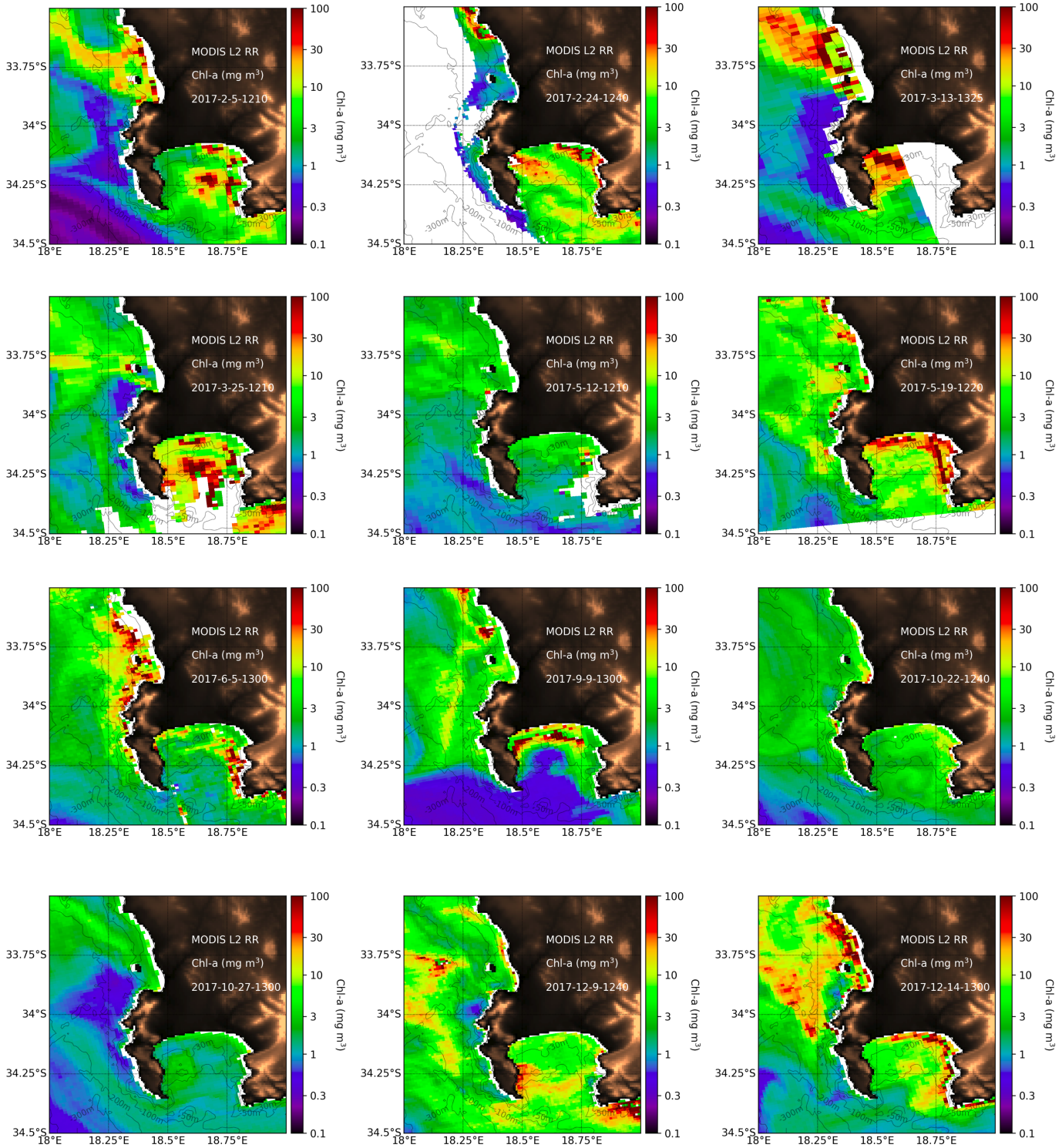


MODIS chlorophyll concentration (Chl-a) maps in mg/m3 for several cases of south-easterly (SE) winds in False Bay and the Cape Peninsula.

# APPENDIX I

## Wind Speed, Sea Surface Temperature and Chlorophyll Concentrations Across False Bay Transect

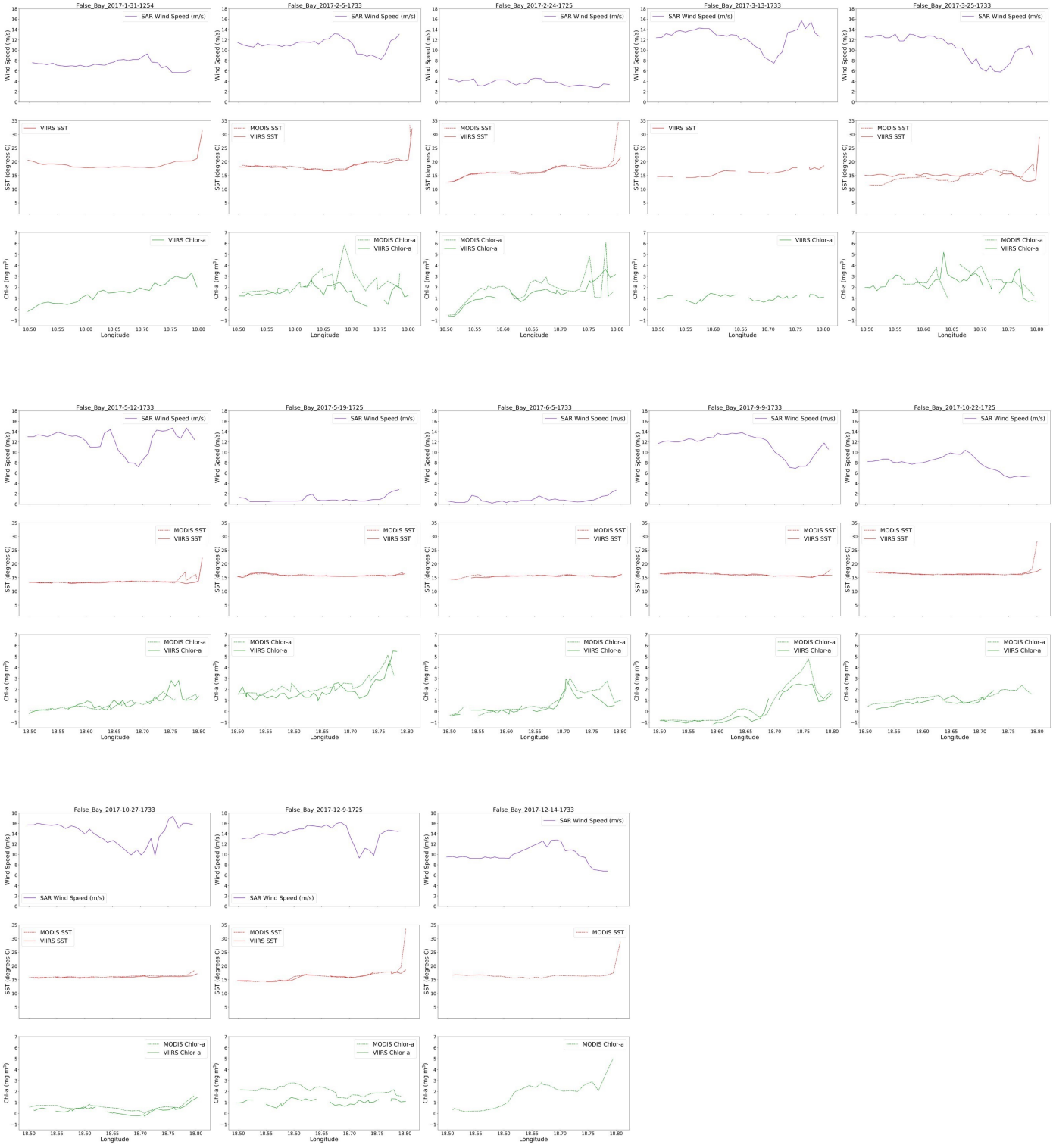


SAR derived wind speed (blue) as well as MODIS (dashed) and VIIRS (solid) sea surface temperature (SST) (red) and chlorophyll concentration (green) along a transect across False Bay. Several case studies are shown for south-easterly (SE) winds.

# APPENDIX J

Wind Speed, Sea Surface Temperature and Chlorophyll Concentrations Across Cape Peninsula Transect


SAR derived wind speed (blue) as well as MODIS (dashed) and VIIRS (solid) sea surface temperature (SST) (red) and chlorophyll concentration (green) along a transect off the northern section of the Cape Peninsula. Several case studies are shown for south-easterly (SE) winds.